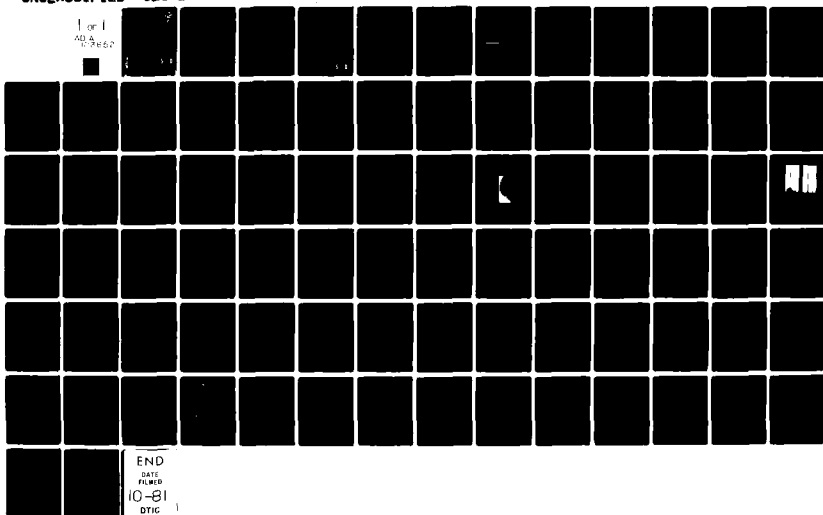


AD-A103 652

UNIVERSITY OF SOUTHERN CALIFORNIA LOS ANGELES CENTER--ETC F/6 20/5  
DEVELOPMENT OF COMPONENTS FOR THE HIGH BRIGHTNESS LASER.(U)  
OCT 80 E GARMIRE  
N61339-77-C-0063  
CLS-2680 NL

UNCLASSIFIED

1 of 1  
AD-A  
03652



END  
DATE  
FILED  
10-81  
DTIC 1

CLS Report 2680

October 1, 1980

AD A 103 652

2  
LEVEL II

DEVELOPMENT OF COMPONENTS FOR THE HIGH BRIGHTNESS LASER

Final Report

Submitted to

PM/TRADE NTEC

By

Elsa Garmire

Center for Laser Studies  
University of Southern California  
University Park  
Los Angeles, California 90007

DTIC  
ELECTE  
S SEP 2 1981 D  
D

81 9 01 113

THIS REPORT IS BASED UPON WORK SUPPORTED BY  
THE ARMY SIMULATION AND TRAINING DEVICE TECHNOLOGY BASE PROGRAM  
UNDER CONTRACT N61339-77-C-0063

DISTRIBUTION UNLIMITED

UNCLASSIFIED

SECURITY CLASSIFICATION OF THIS PAGE (When Data Entered)

| REPORT DOCUMENTATION PAGE   |  | READ INSTRUCTIONS BEFORE COMPLETING FORM |
|---|--|--|
| 1. REPORT NUMBER<br>CLS Report 2680   | 2. GOVT ACCESSION NO.<br>AD-A103 652                                     | 3. RECIPIENT'S CATALOG NUMBER            |
| 4. TITLE (and Subtitle)<br>DEVELOPMENT OF COMPONENTS FOR THE HIGH BRIGHTNESS LASER  | 5. TYPE OF REPORT & PERIOD COVERED<br>FINAL 5/77 - 6/80                  |  |
| 7. AUTHOR(s)<br>10<br>Elsa Garmire  | 6. PERFORMING ORG. REPORT NUMBER<br>CLS-2680                             |  |
| 9. PERFORMING ORGANIZATION NAME AND ADDRESS<br>Center for Laser Studies<br>University of Southern California<br>University Park, Los Angeles, CA 90007  | 10. PROGRAM ELEMENT, PROJECT, TASK AREA & WORK UNIT NUMBERS<br>11 111-89 |  |
| 11. CONTROLLING OFFICE NAME AND ADDRESS<br>PM/TRADE<br>NTEC<br>Orlando, Florida 32813   | 12. REPORT DATE<br>October 1, 1980                                       |  |
| 14. MONITORING AGENCY NAME & ADDRESS (if different from Controlling Office)<br>971 N. 1st St.<br>Phoenix, AZ 85004  | 13. NUMBER OF PAGES<br>79  |  |
| 15. SECURITY CLASS. (of this report)  |  |  |
| 15a. DECLASSIFICATION DOWNGRADING SCHEDULE  |  |  |
| 16. DISTRIBUTION STATEMENT (of this Report)<br><div style="border: 1px solid black; padding: 5px; text-align: center;"><b>DISTRIBUTION STATEMENT A</b><br/>Approved for public release;<br/>Distribution Unlimited</div>  |  |  |
| 17. DISTRIBUTION STATEMENT (of the abstract entered in Block 20, if different from Report)  |  |  |
| 18. SUPPLEMENTARY NOTES   |  |  |
| 19. KEY WORDS (Continue on reverse side if necessary and identify by block number)<br>Lasers, Integrated Optics, Distributed Feedback, Distributed Bragg Reflector (DBR) Lasers, gratings, Amplifiers, GaAs lasers, GaAs Amplifiers, Single Mode Lasers   |  |  |
| 20. ABSTRACT (Continue on reverse side if necessary and identify by block number)<br>In 1979 DBR lasers were fabricated and their properties studied. Further investigations were undertaken of the beam expander, to determine its potential for the high brightness laser. From this data it was determined that a design change for the high brightness laser is required. This design change is described.<br><br>In addition, measurements were made on laser amplification to compare this method of achieving higher power compared to the coupled diode arrays.<br>(cont'd on back) |  |  |

DD FORM 1 JAN 73 1473

UNCLASSIFIED

SECURITY CLASSIFICATION OF THIS PAGE (When Data Entered)

5/15-1

Unclassified

SECURITY CLASSIFICATION OF THIS PAGE(When Data Entered)

20. Abstract (Cont'd)

Finally, as a spin-off of this research, a new design for a single mode laser was discovered, using the active/passive laser, a configuration which was fabricated as a first step toward fabrication of DBR lasers. Each of these research efforts are described in this report.

Monolithic integration of the necessary components on one substrate for the high brightness laser has been hindered by problems in material and fabrication uniformity. This will be described, and projections for future development will be outlined.

UNCLASSIFIED

SECURITY CLASSIFICATION OF THIS PAGE(When Data Entered)

## DEVELOPMENT OF COMPONENTS FOR THE HIGH BRIGHTNESS LASER

E. Garmire

### ABSTRACT

In 1979 DBR lasers were fabricated and their properties studied. Further investigations were undertaken of the beam expander, to determine its potential for the high brightness laser. From this data it was determined that a design change for the high brightness laser is required. This design change is described.

In addition, measurements were made on laser amplification to compare this method of achieving higher power compared to the coupled diode arrays.

Finally, as a spin-off of this research, a new design for a single mode laser was discovered, using the active/pассив laser, a configuration which was fabricated as a first step toward fabrication of DBR lasers. Each of these research efforts are described in this report.

Monolithic integration of the necessary components on one substrate for the high brightness laser has been hindered by problems of material and fabrication uniformity. This will be described, and projections for future development will be outlined.

|   |                          |
|---|--------------------------|
| Accession For   |                          |
| NTIS  | CR481                    |
| DTIC TAB  | <input type="checkbox"/> |
| Unannounced   | <input type="checkbox"/> |
| Justification   |                          |
| Doc. No. (FL-89, R81-1900,<br>By <del>DTIC</del> 20 July 81) on<br>Distribution/ file |                          |
| Availability Codes  |                          |
| Avail and/or<br>Dist  | Special                  |
| A   |                          |

DTIC  
ELECTE  
S SEP 2 1981 D  
D

## TABLE OF CONTENTS

|  | Page |
|--|------|
| Abstract . . . . .   | i    |
| I. Introduction . . . . .  | 1    |
| II. DBR Laser Properties . . . . .   | 5    |
| III. Waveguide Beam Expansion . . . . .  | 23   |
| IV. New Designs for the High Brightness Laser . . . . .                              | 38   |
| V. Materials and Fabrication Studies . . . . .                                       | 41   |
| VI. Amplifier Studies . . . . .  | 45   |
| VII. Single Mode Three-Mirror Lasers Using Integrated Optics<br>Techniques . . . . . | 66   |
| VIII. Projections for the Future. . . . .  | 77   |
| Table of Publications Supported on this Contract                                     |      |

## I. INTRODUCTION

This report describes the continuation research toward developing high brightness laser (HBL) sources. In the proposal for this work, we expected to obtain DBR lasers by December, 1978. In fact, we fabricated our first successful DBR lasers in April, 1979, and made extensive studies of their properties. These studies are included in Chapter II.

We found that further studies of the beam expander were necessary and they led to necessary design changes for the HBL. These studies are outlined in Chapter III, and the new HBL designs are described in Chapter IV.

Because of continuing materials and fabrication problems and turnover of personnel, monolithic integration of the DBR laser and beam expander was not achieved during 1979 nor during the no-cost extension into 1980. A description of the research during the period of the contract for continuation research, our investigation into and development of methods for overcoming these problems is contained in Chapter V. Projections for expected development of the monolithic integration for the HBL are contained in Chapter VIII.

Chapter VI contains studies of laser amplification, in accordance with the proposal, and Chapter VII contains our unexpected development of a new technique for fabricating single mode lasers, a fortunate spin-off of this research.

The rest of this introduction contains a brief outline of the technical concept of the high brightness laser.

The Distributed Bragg Reflector (DBR) laser is the light source compatible with monolithic integrated optics which will be used with the high brightness laser. In the DBR laser one or both cleaved endfaces of a typical double heterostructure laser is replaced by a corrugation at half the wavelength of light in the GaAs. This grating acts as a retro-reflector and replaces the cleave as a laser cavity mirror. The DBR laser can be used as an integrated optics light source for integrated optical circuits.

In this report we describe theory and experiments on the DBR laser and on the use of the Distributed Bragg Deflector (DBD) to act as a grating beam expander. The DBD is a corrugation placed at an angle with respect to light emitted from the DBR laser. This grating serves to deflect the incident light through an angle in a distributed fashion, thereby expanding the light beam. This is shown schematically in Fig. 1. The expanded beam travels within the plane of the waveguide and is the basis of several optical circuits, which have application in optical signal processing and optical communications and is the basis for the high brightness laser, being developed on this contract.

In the high brightness laser (HBL) the beam expander is combined with an output coupler to produce a low beam-divergence laser. This is shown in Fig. 2. The output coupler is a grating corrugation with a spacing which is equal to the wavelength of the propagating light. A grating of this spacing

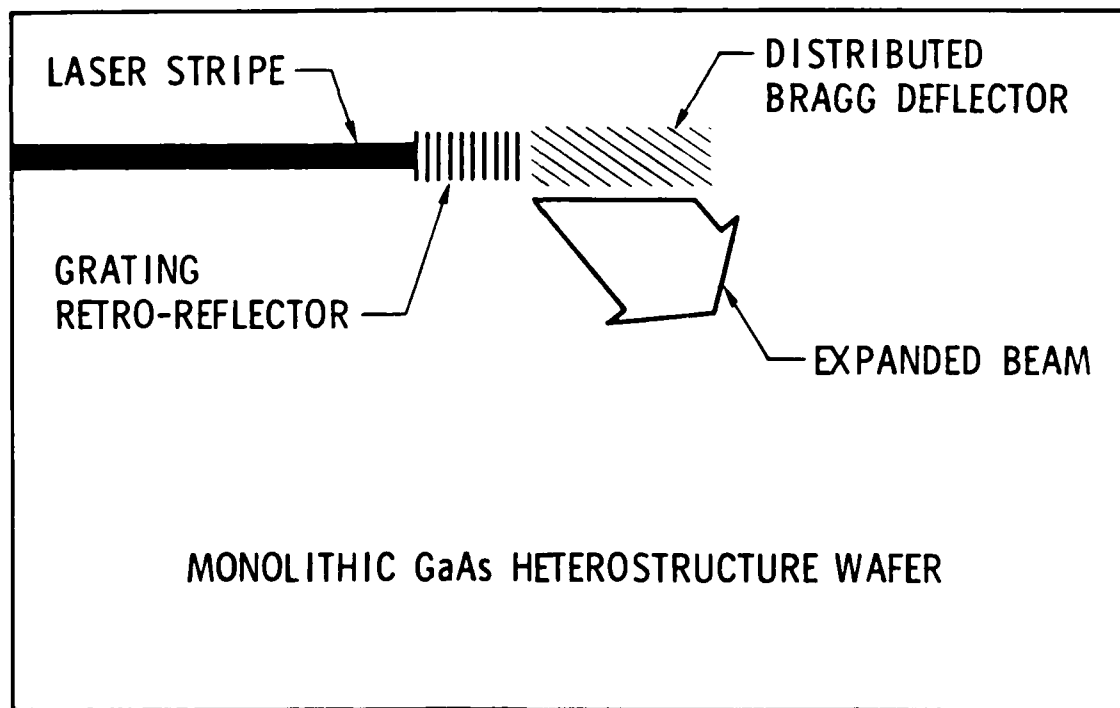


**Figure 1** Distributed Bragg Deflector, acting to expand the beam from a DBR laser into a wide beam within the plane of the waveguide for use in optical signal processing.

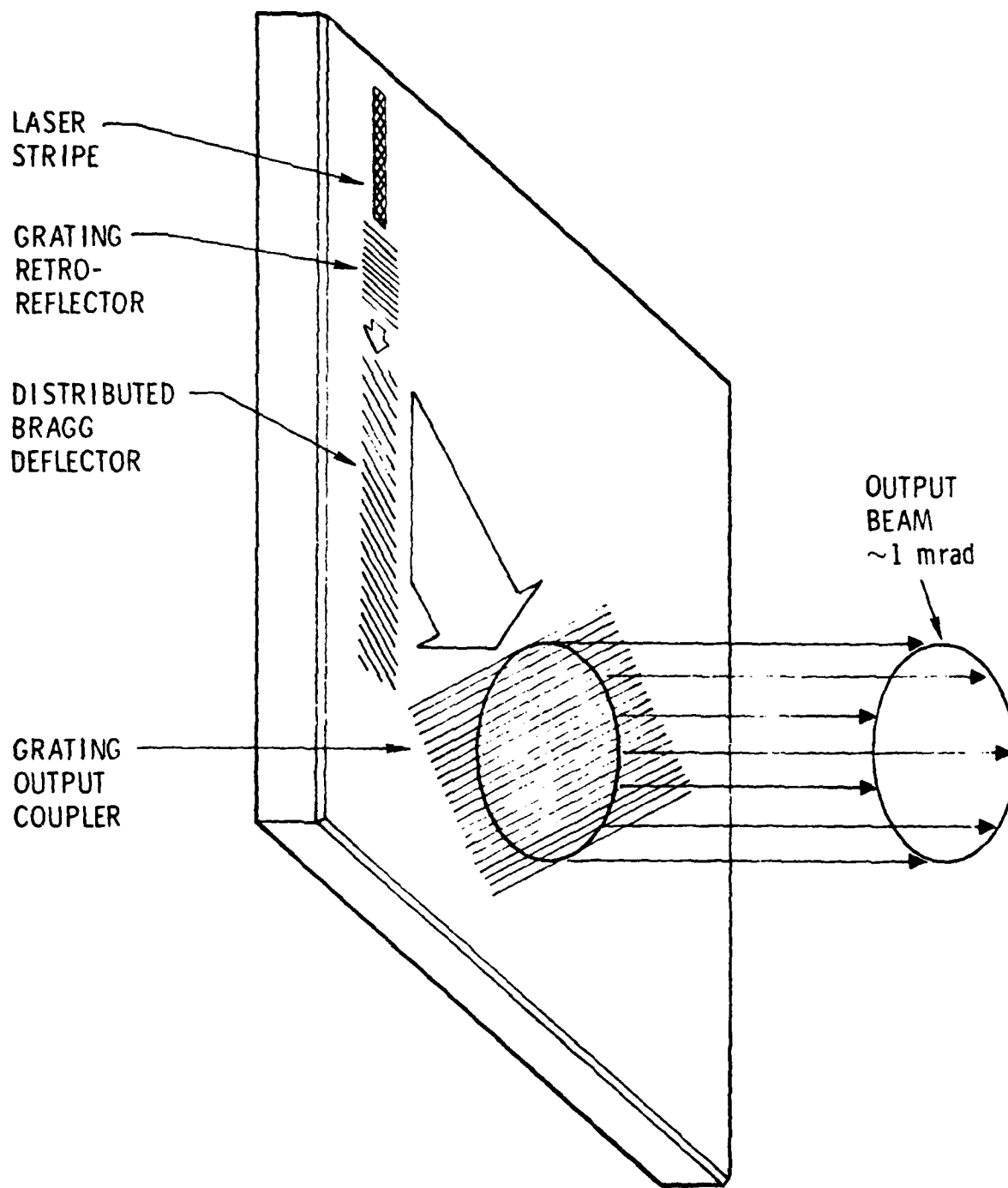


Figure 2 Low beam-divergence laser. The gratings act as an integrated optical spatial filter and telescope.

deflects the beam out of the plane of the waveguide and into free space, propagating normal to the plane of the waveguide. Since the deflection is distributed, the beam is expanded by this deflection, and, for apertures about 1 mm in diameter, a diffraction-limited beam 1 mrad in divergence angle will be created. The combination beam expander and output coupler serve as integrated optical telescope and spatial filter. This HBL has applications in point-to-point optical communication systems, as well as in training devices.

Applications requiring more power can use the DBD as a power combiner for several laser stripes, two designs of which are shown in Figs. 3 and 4. In design studies, it has been shown that 1 Watt with a 1 mrad radiance angle is possible. The changes in this design over the original proposed design will be discussed in this report.

In Chapter II we discuss experiments performed on DBR laser, with emphasis on its usefulness for the high brightness laser monolithic design. In Chapter III we discuss the beam expander, and how its properties have put a constraint on the design of the HBL. In Chapter IV we discuss the new design geometries shown in Fig. 3 and 4. In Chapter V we discuss the problems we have faced regarding materials and fabrication, which have kept us from completing the monolithic integrating of the HBL. Nothing in our research has discouraged us from faith in the ultimate concept. However, we have discovered that the materials and fabrication problems are a lot more difficult than we expected. We anticipate continued research toward the HBL, but over a much longer time-scale for completion of the project than originally projected.

### III. DBR LASER PROPERTIES

The cross section geometry of the DBR lasers which were fabricated is shown in Fig. 5. The gratings were third order, and the laser region was a large optical cavity. The layer structure shown was not optimum, because the waveguide region was thicker than desired, but was the best material available at the time. Thresholds of these first diodes were typically  $3.5 \times 10^4$  Amps/cm<sup>2</sup> and the output was TE-polarized.

Measurements were made of the front-to-rear power ratio of DBR lasers of differing lengths to determine the coupling coefficient of the grating and to

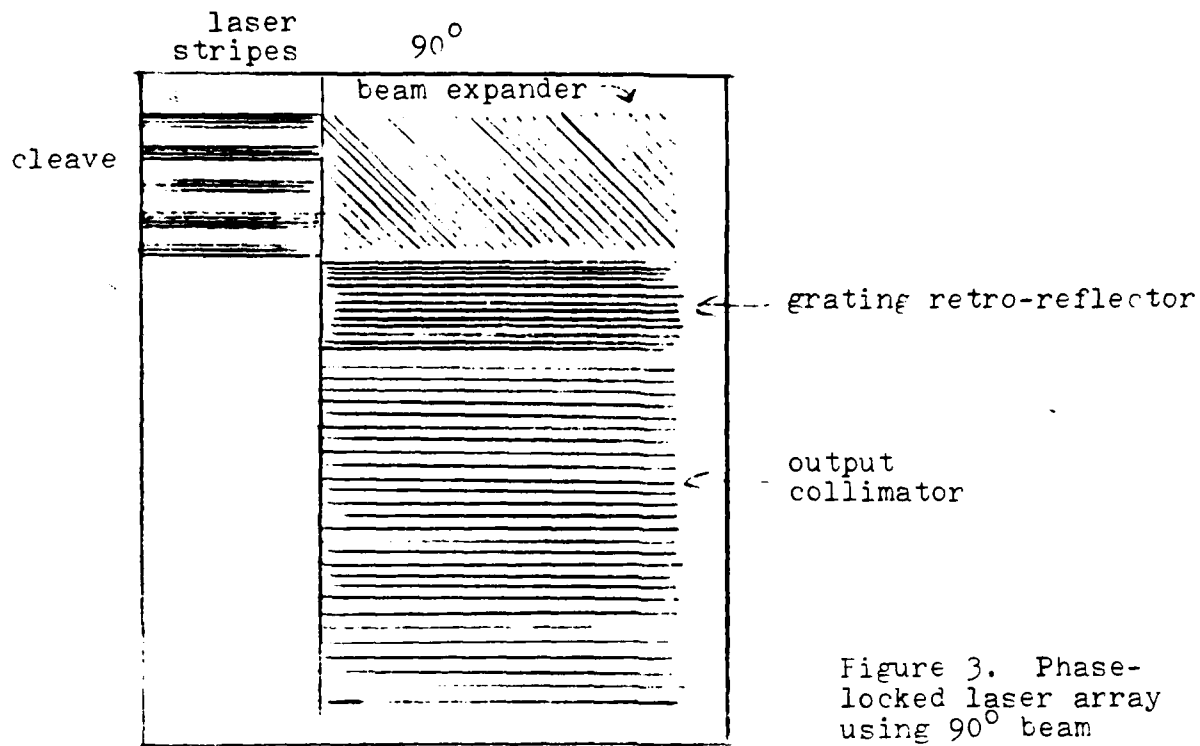


Figure 3. Phase-locked laser array using  $90^\circ$  beam expander.

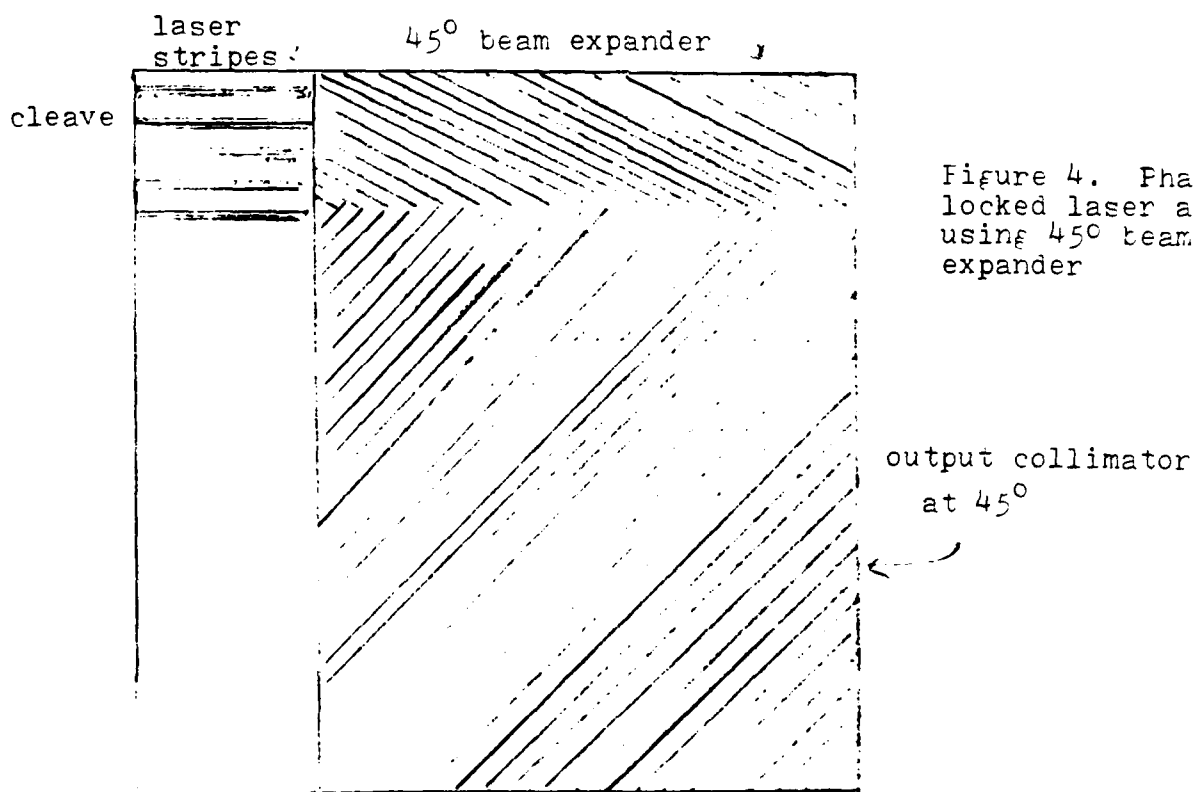


Figure 4. Phase-locked laser array using  $45^\circ$  beam expander

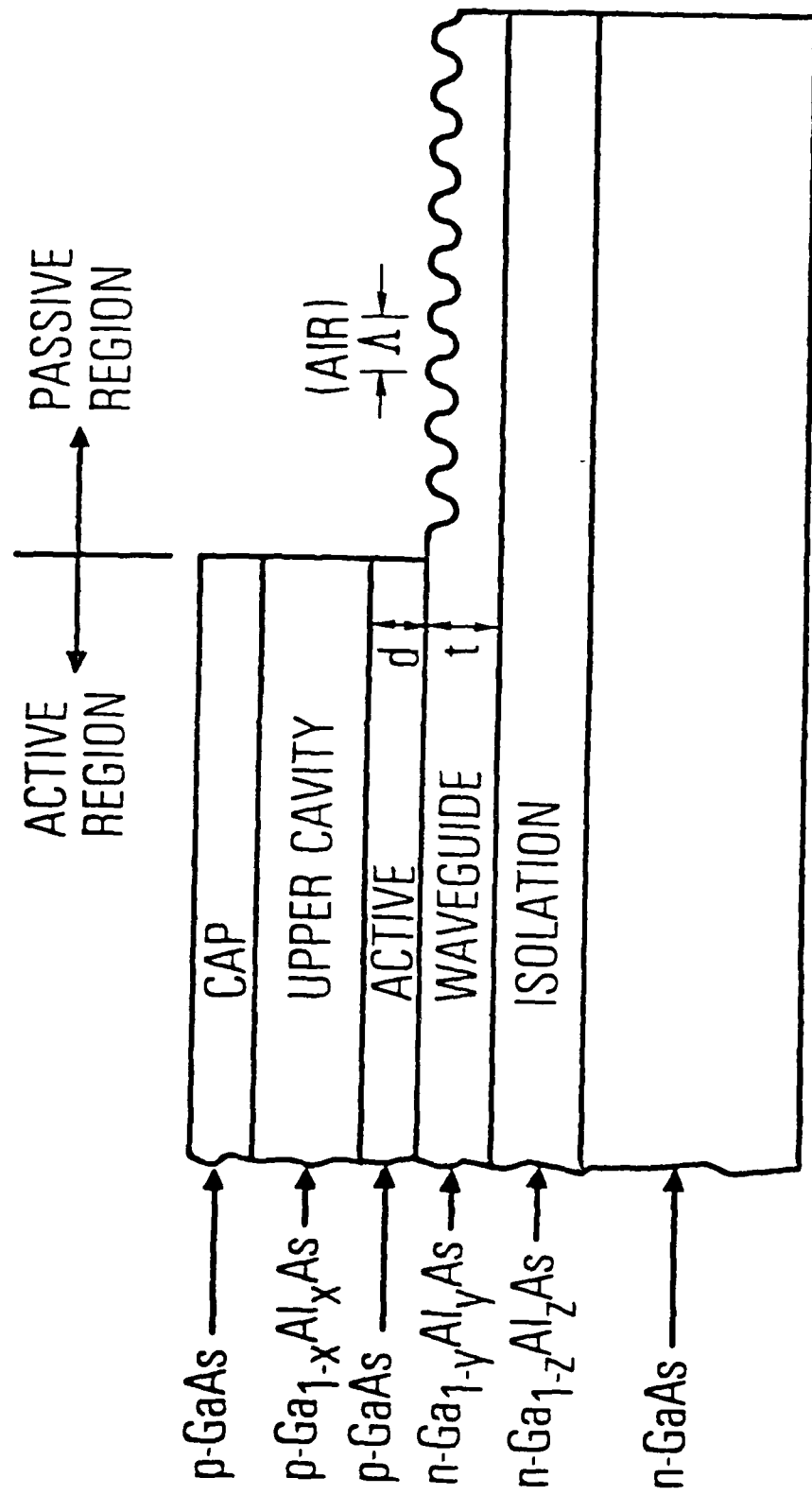


Figure 5 Geometry of the DBR laser fabricated and studied. The important parameters are  $d = 0.25 \mu\text{m}$ ,  $t = 1.68 \mu\text{m}$ ,  $x = 0.26$ ,  $y = 0.1$ ,  $z = 0.34$ ,  $\lambda = 0.36$ .

check for its reproducibility. Two devices were compared in detail; the data is shown in Table I.

Table I

Data to determine coupling coefficient of gratings in DBR lasers

| Sample Number                      | $g^9$              | $g^5$             |
|------------------------------------|--------------------|-------------------|
| Power out grating (mW)             | 1                  | 0.5               |
| Power out cleave (mW)              | 30                 | 10                |
| Power ratio (grating to cleave), T | 0.03               | 0.05              |
| $\ln T/4 = -5.0$                   | -4.4               |                   |
| Grating Length                     | 1000 $\mu\text{m}$ | 464 $\mu\text{m}$ |
| $K (\mu\text{m}^{-1})$             | 0.0024             | 0.0047            |
| $L_g = (2K)^{-1}$                  | 205 $\mu\text{m}$  | 106 $\mu\text{m}$ |

It can be seen that only a small fraction of the light was transmitted through the grating. Clearly these DBR lasers had gratings which were longer than desirable for the HBL. However, we can use this data to compare to theoretical estimates and design the proper geometry.

According to the theory, a grating retro-reflector of length L on resonance has the following behavior for transmission and reflection:

Transmission:

$$T = \frac{1}{\cosh^2 KL} \quad (1)$$

Reflection:

$$R = \frac{\sinh^2 KL}{\cosh^2 KL} \quad (2)$$

When  $KL \gg 1$ :

$$T = 4e^{-2KL}, \quad R = 1 - T. \quad (3)$$

The coupling coefficient was determined from Eq. (3) using the fact that the front-to-back power ratio will be the same as the transmission of the

grating. The results are shown in Table 1. Although the values of  $K$  differ by a factor of two, we feel this is well within experimental error. The average coupling coefficient is  $K = 0.0035 \mu\text{m}^{-1}$ . We now compare these measurements with theoretical expectations.

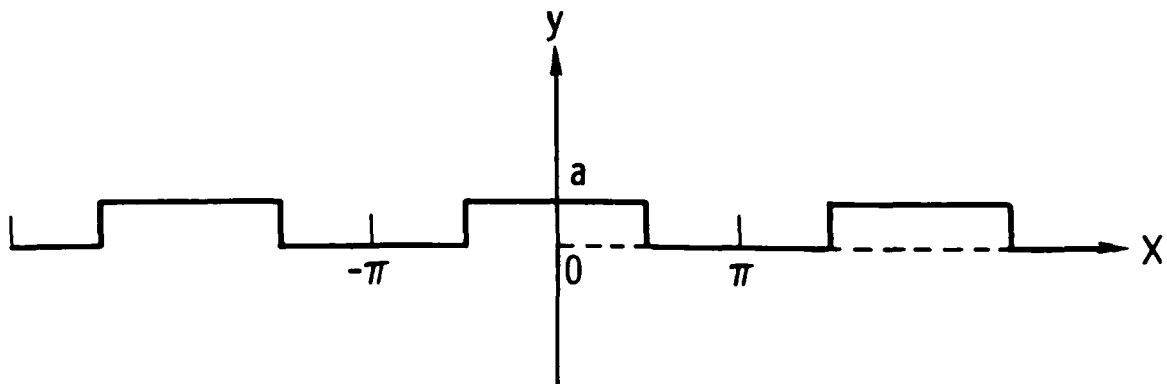
Coupled mode theory predicts that a corrugated waveguide couple forward and backward waveguide modes with a coupling coefficient  $K$ . Light originally travelling forward transfers to the backward wave exponentially with length, with a coefficient given by  $K$ . Thus the effectiveness of a grating can be described by describing its coupling coefficient. For square corrugations of depth  $d$  the coupling coefficient is <sup>(1)</sup>

$$K = \frac{2\pi^2 (n^2 - 1)}{3 m \lambda n} \left( \frac{d}{t} \right)^3. \quad (4)$$

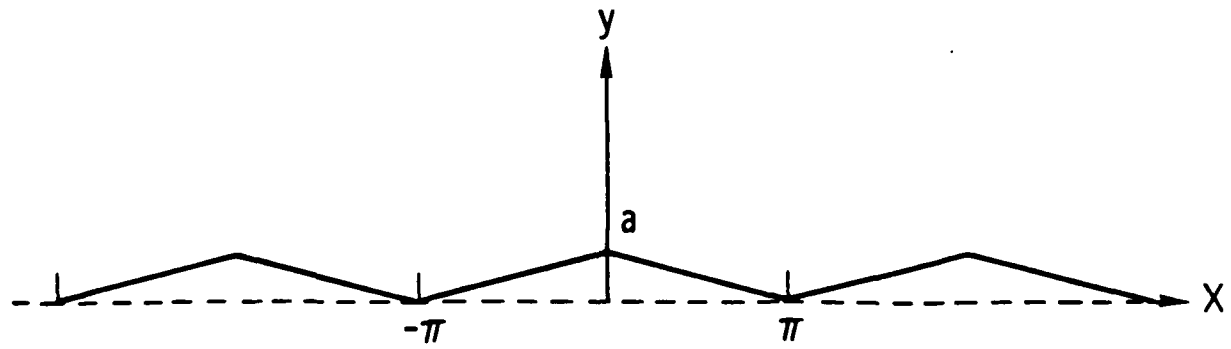
where  $n$  is the refractive index of the guide,  $t$  is the thickness of the waveguide and  $m$  is the mode number. A related parameter is the characteristic distance at which the power in the initial mode decreases by a factor of  $1/e$ . This characteristic length is given by  $L_g = (2K)^{-1}$ . The experimental grating looked more like triangular teeth than square teeth, however. The comparison between square and triangular shapes may be made by comparing the Fourier transforms for the third order coefficients for square and triangular shapes. Using the calculations shown in Fig. 6, we see that the polarization induced by a triangular grating will be  $2/3$  that induced by the step index. Thus we expect the grating coupling coefficient to be

$$K = \frac{4\pi^2 (n^2 - 1)}{9 m \lambda n} \left[ \frac{d}{t_e} \right]^3 \quad (5)$$

where we have taken Eq. 4, multiplied by  $2/3$  and used  $t_e$ , the effective guided mode thickness, instead of  $t$ , for guides which are not infinitely well confining.



$$F = \int_{-\pi}^{\pi} y(x) \cos 3x \, dx = a \int_{-\pi/2}^{\pi/2} \cos 3x \, dx = \frac{2a}{3}$$



$$F = \int y(x) \cos 3x \, dx = -2a \int_0^{\pi} x \cos 3x \, dx = \frac{4a}{9}$$

Figure 6 Geometry and calculations used to determine effectiveness of triangular teeth compared to square teeth in producing feedback.

From SEM photographs of the grating, we estimate  $d = \Lambda/3$ ,  $t = 1.68 \mu\text{m}$ ,  $\Lambda = \text{the grating periodicity} = 0.36\mu\text{m}$ . The grating was used in third order, and the refractive index of GaAs at  $0.88 \mu\text{m}$  is 3.59. These numbers give the theoretically expected coupling coefficient of  $K = 0.0059\mu\text{m}^{-1}$ . In order to calculate this number, it was required to know the effective guide width. This was determined by solving the eigenvalue equation for the waveguide to determine the exponential profile outside of the guide,  $\gamma$ , and calculate  $t_e = t + 1/\gamma$ . For the DBR lasers, the  $V$  parameter for the waveguide was  $\Delta k_o^2 t^2 = 146$ , resulting in two modes, given by the following eigenvalue equation:

$$\tan u = - \left( \frac{146}{2} - 1 \right)^{-1/2} \quad \text{where } u = k_t t$$

The solutions are  $k_t t = 2.9, 5.8$ , and give  $\gamma t = 12$  for both modes. This makes the effective thickness  $= 1.75 \mu\text{m}$  for both. This is the value used in Eq. (5) to determine the theoretical coupling coefficient. The calculated value of 0.0059 agrees within experimental error with the measured value of .0035. The agreement between theory and experiment allows us to predict behavior for other waveguides. For example, material with waveguide thickness of  $0.6 \mu\text{m}$  should yield devices with coupling coefficients as much as eight times larger.

Optimum energy transfer will occur from the DBR laser to the rest of the HBL circuit when the transmission of the grating is  $\sim 50\%$ . For the measured value of  $K = 0.0035 \mu\text{m}^{-1}$  this corresponds to a DBR retroreflector grating with  $KL = 0.63$ , or a length of  $180 \mu\text{m}$ . This is 2.5 times shorter than the shortest gratings we tried.

Other properties relevant to DBR lasers as sources for fiber optics, high brightness lasers and optical signal processing by monolithic integrated optics were investigated. These include the spectrum, total power, the P-I characteristics, and the beam divergences in both planes, including whether or not the light was diffraction limited. The results are summarized here. A typical spectrum of a DBR laser is shown in Fig. 7. First, in order to prove that the laser action occurred from the grating and not from spurious

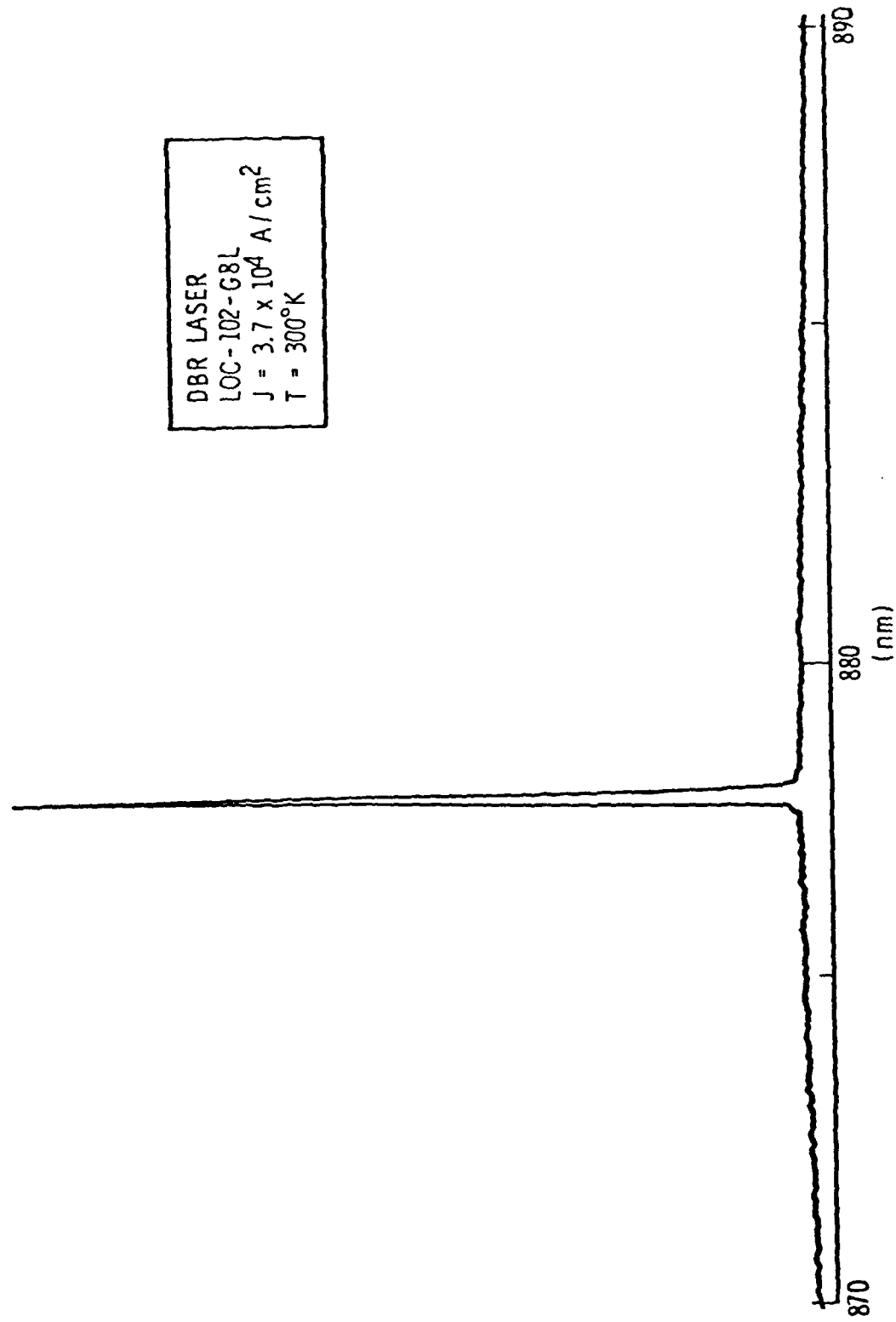


Figure 7 Spectrum of typical DBR laser.

reflections the following tests were applied. First, it was observed that the spectrum was a single mode. Comparable spectra for Fabry-Perot lasers from the same material were multimode, as shown in Fig. 8. Secondly, a DBR laser which operated at room temperature was cooled to liquid nitrogen temperature, and laser action ceased, since the reflectivity of the grating was no longer at the frequency of the fluorescence. This is in contrast to Fabry-Perot lasers whose frequency shifts and threshold lowers with temperature.

In some of the diodes two lines occurred, as shown in Fig. 9. This occurred because the waveguide was sufficiently thick that not only the lowest even mode, but also the lowest odd mode could be confined in the passive region. These modes are shown in Fig. 10, and occur in the following way.

The laser wavelength is determined by the condition that the corrugation spacing is in resonance with the longitudinal propagation vector: i.e.  $k_z = 3 \pi/\Lambda$ . However, the different modes have different propagation constants since the transverse propagation constant is different for each mode. The dispersion relation thus becomes

$$k_z^2 = n_g^2 k_0^2 - \left( \frac{(m+1)\pi}{t_e} \right)^2. \quad (6)$$

To get a simple expression for the difference in frequencies for DBR laser lines operating on different waveguide modes, assume that the effective waveguide thickness is independent of mode, that the refractive index does not depend on frequency, and that the difference in wavelength between the two laser modes is much less than the wavelength. Then the equation for laser wavelength, given by

$$\left( \frac{3}{\Lambda} \right)^2 = \frac{4n^2}{\lambda^2} - \left( \frac{m+1}{t_e} \right)^2$$

can be differentiated, yielding,

$$\Delta\lambda = \frac{3\lambda^3}{8t_e^2 n_g^2}. \quad (7)$$

The refractive index which comes into the calculation of laser modes is the effective index:

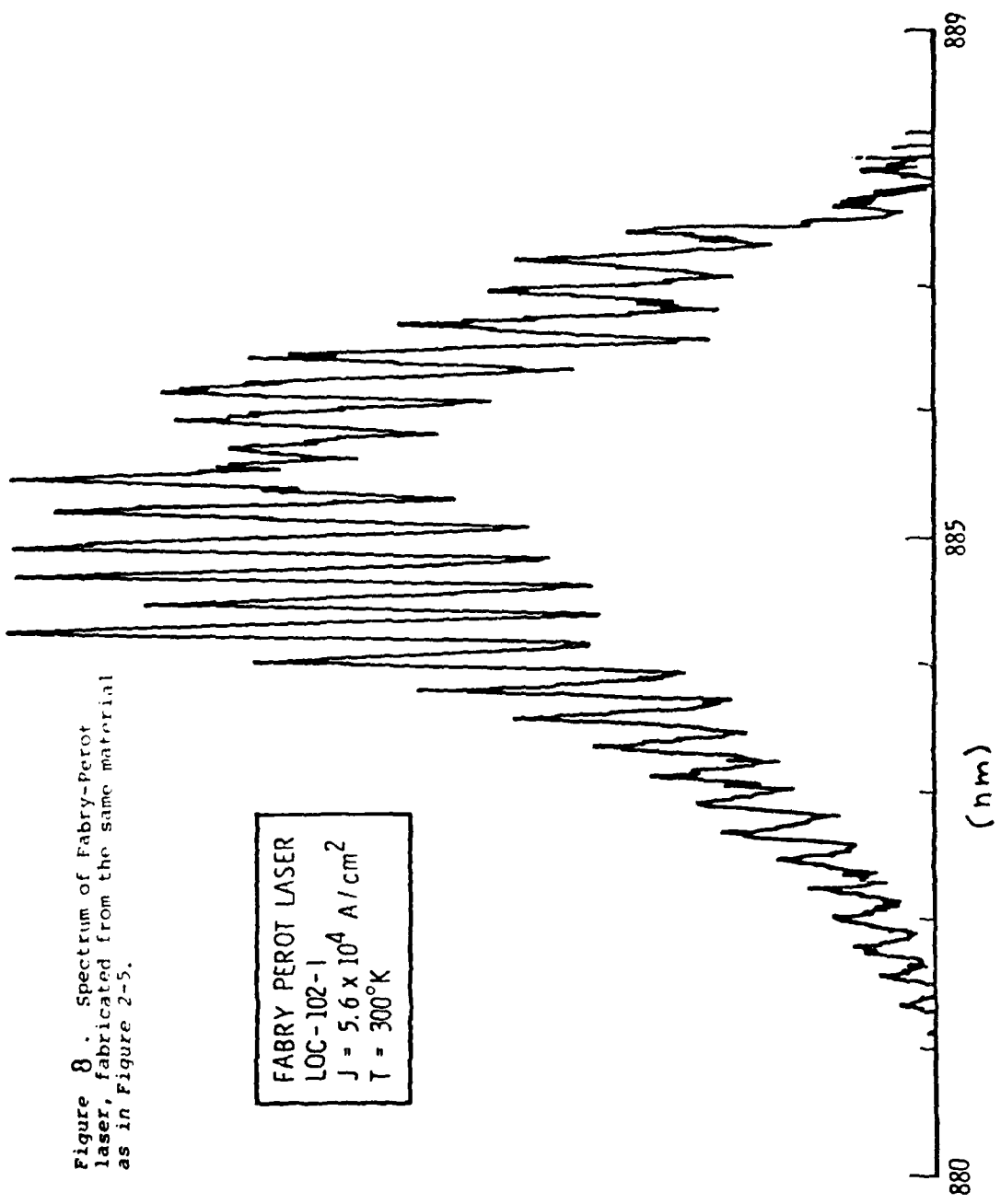


Figure 8: Spectrum of Fabry-Perot laser, fabricated from the same material as in Figure 2-5.

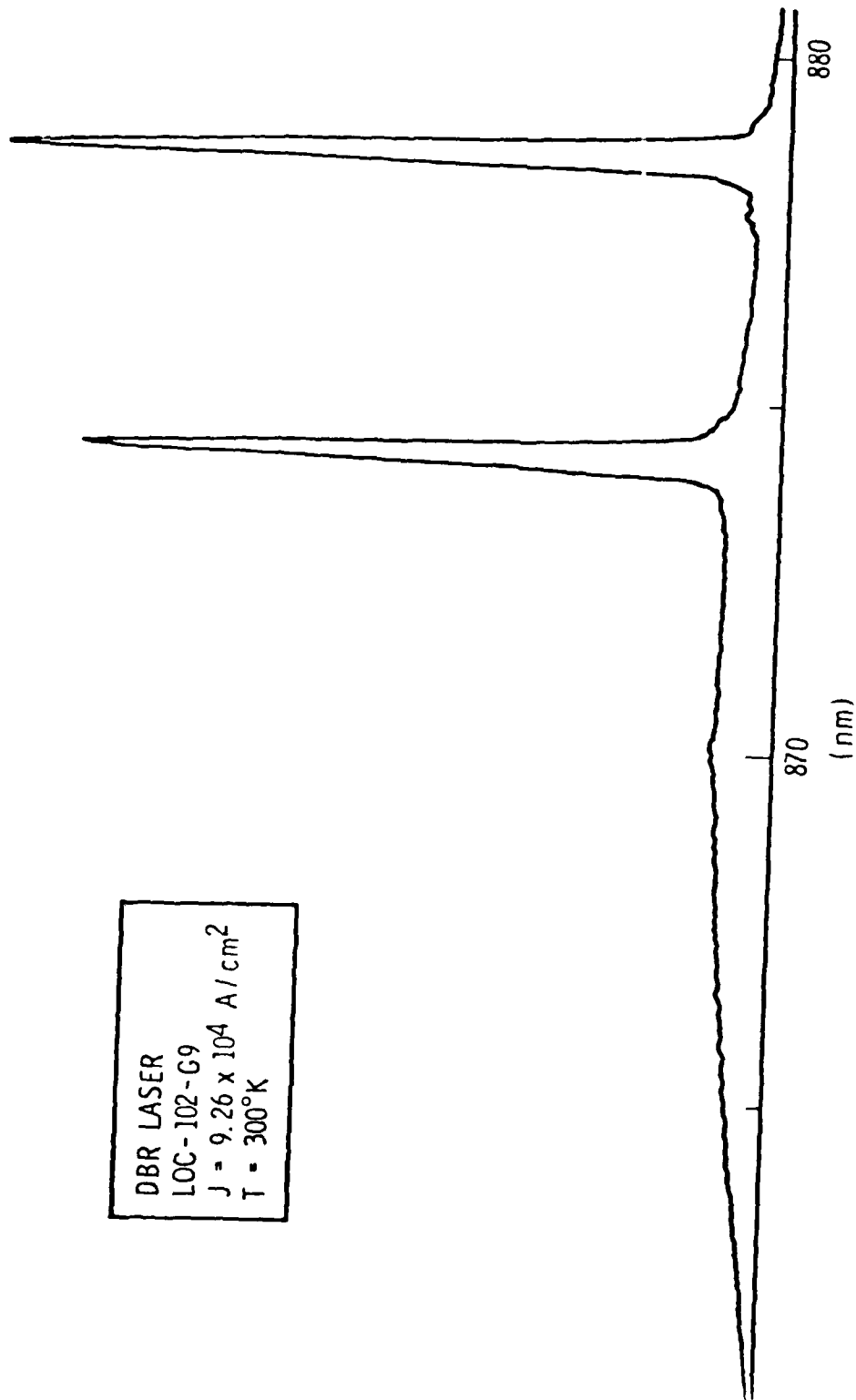


Figure 9 Spectrum of DBR laser which supports two waveguide modes and therefore has two oscillation frequencies.

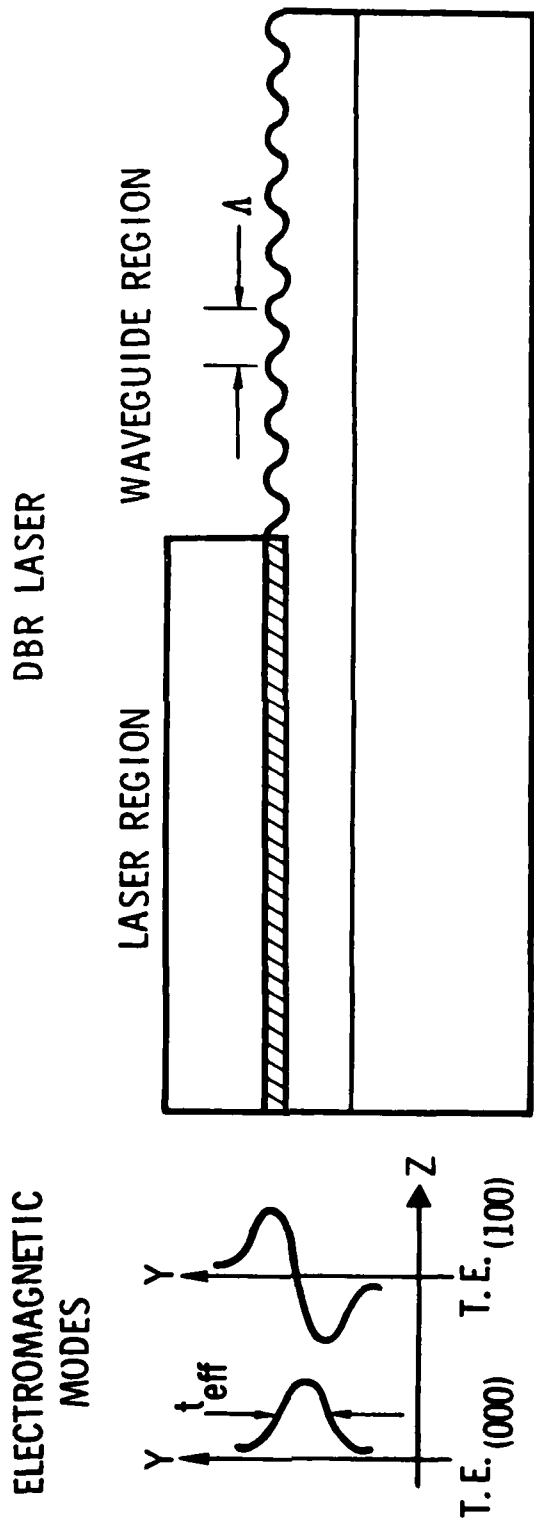


Figure 10 DBR laser geometry, showing the two TE modes which exist in the DBR laser when the waveguide layer is fairly thick. Each of these modes has a different longitudinal propagation constant and therefore oscillates at a different frequency.

$$n_{\text{eff}} = n + v \frac{dn}{dv} \approx 4.8$$

For an effective waveguide thickness of 1.75  $\mu\text{m}$ , the difference in wavelength between modes should be 35 $\text{\AA}$ . In devices tested, the actual difference between modes was 40 $\text{\AA}$ . We consider this good agreement, to within the accuracy to which  $t_e$  is known. Finally, as further check on this explanation of the two output frequencies, we measured their far field mode profiles separately. We observed that the longer wavelength oscillation was in the lowest order spatial mode, while the shorter wavelength oscillation had a double-humped far field profile, proving that it was indeed oscillating in the higher order waveguide mode.

The linewidths just above laser threshold were typically about 1 $\text{\AA}$ . Diode G8, shown in Fig. 7, had a width of about 1.1  $\text{\AA}$ , and diode G9, shown in Fig. 11a, had a width of 1.6  $\text{\AA}$ . The apparent linewidth broadened slightly with pumping, as shown in Fig. 11b, in which diode g5 is pumped three times threshold. The line had broadened to about 3  $\text{\AA}$ . It was observed on the oscilloscope that the frequency changed during the 100 nsec of the input pulse. The broadening was a chirp effect due to heating in the junction. Such effects have been seen before in Fabry-Perot diodes, but here are much smaller because of the smaller temperature sensitivity of DBR lasers.

Diode g9 had a complicated behavior, since the two frequencies corresponding to two guided modes occurred at high pumping rates. It was observed that at low excitation levels the shorter wavelength was the strongest peak and the longer wavelength occurred only during the initial portion of the pulse. Evidently heating caused the resonance condition to change and near the end of the pulse the shorter wavelength had a lower threshold and was the only frequency above threshold. This data demonstrates that even when a grating is used, it is possible to get several wavelengths oscillating, not necessarily simultaneously in time within the laser. Clearly DBR diodes must be optimized to have well-behaved results.

The complexity of this device can be seen from the P-I curve (Fig. 12), which are filled with kinks. The DBR laser causes only one or two frequencies to oscillate, but does not necessarily improve P-I characteristics over Fabry-Perot lasers.

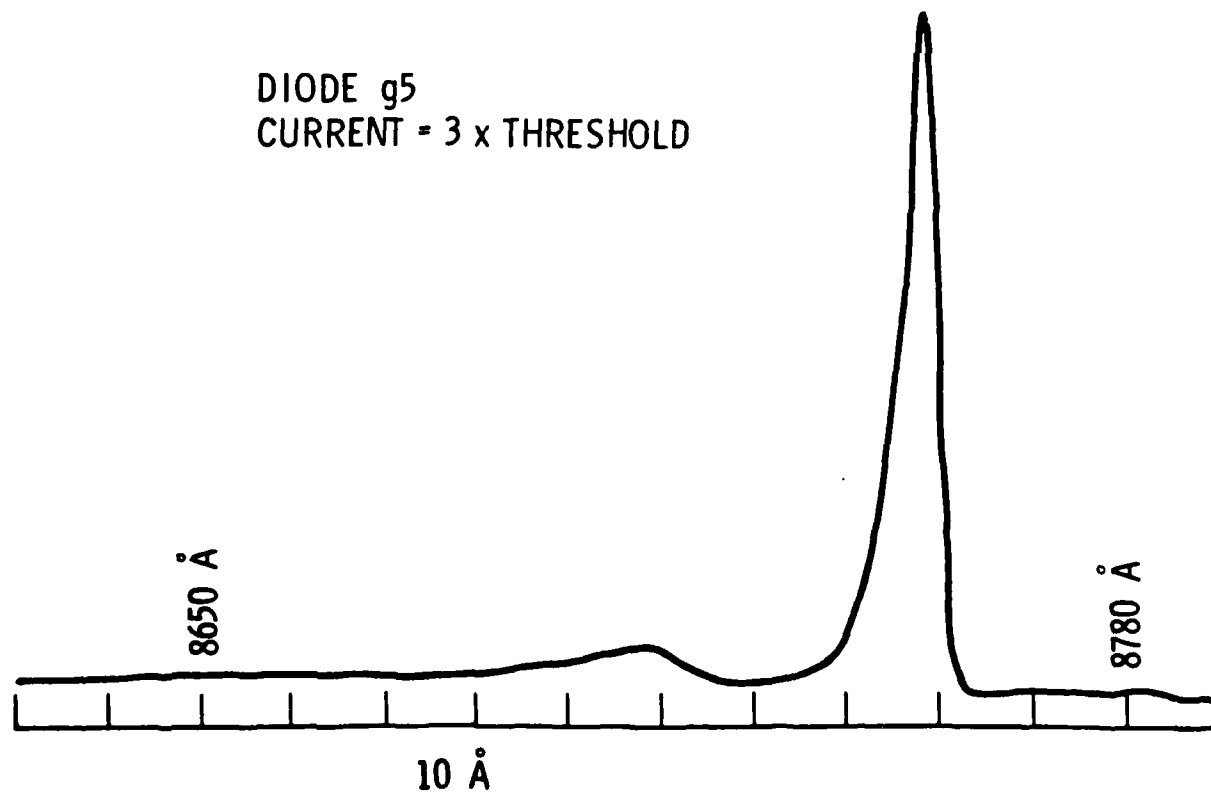
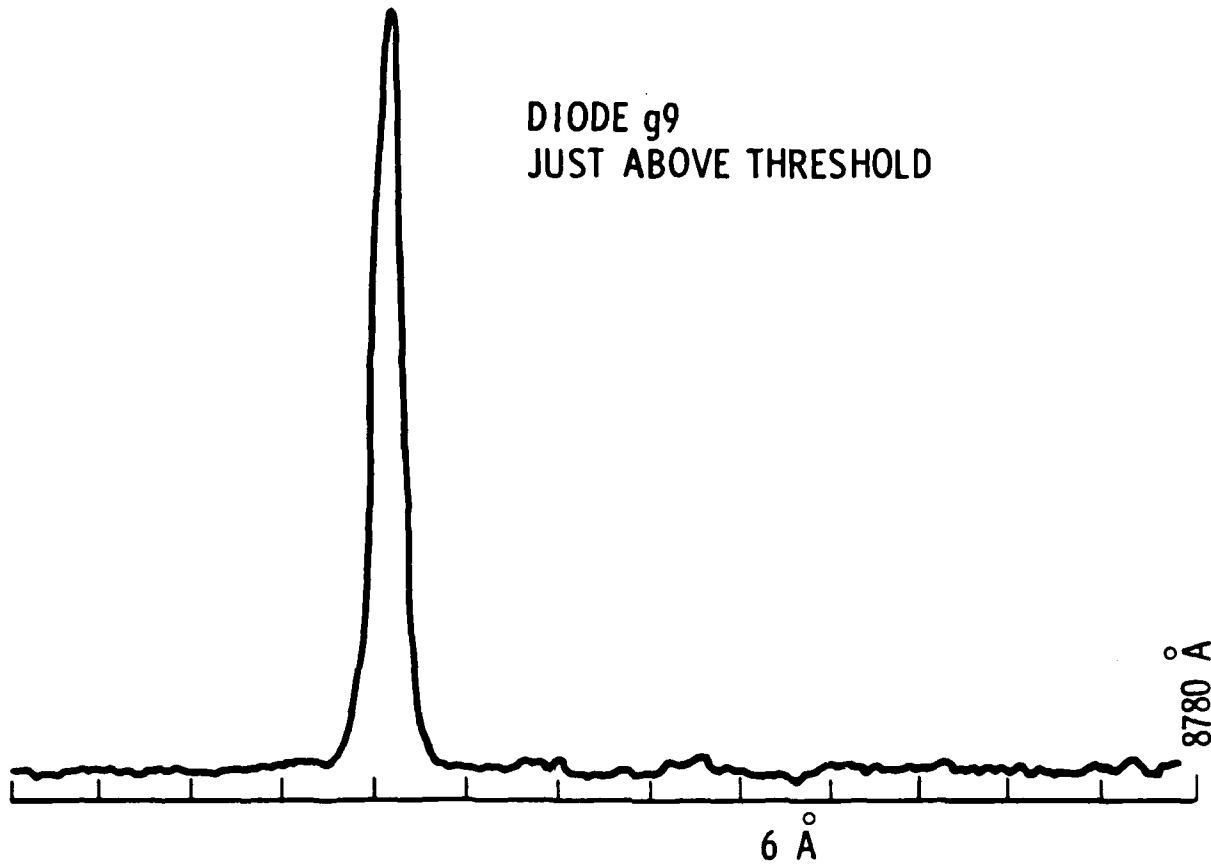


Figure 11 Spectra of two DBR lasers

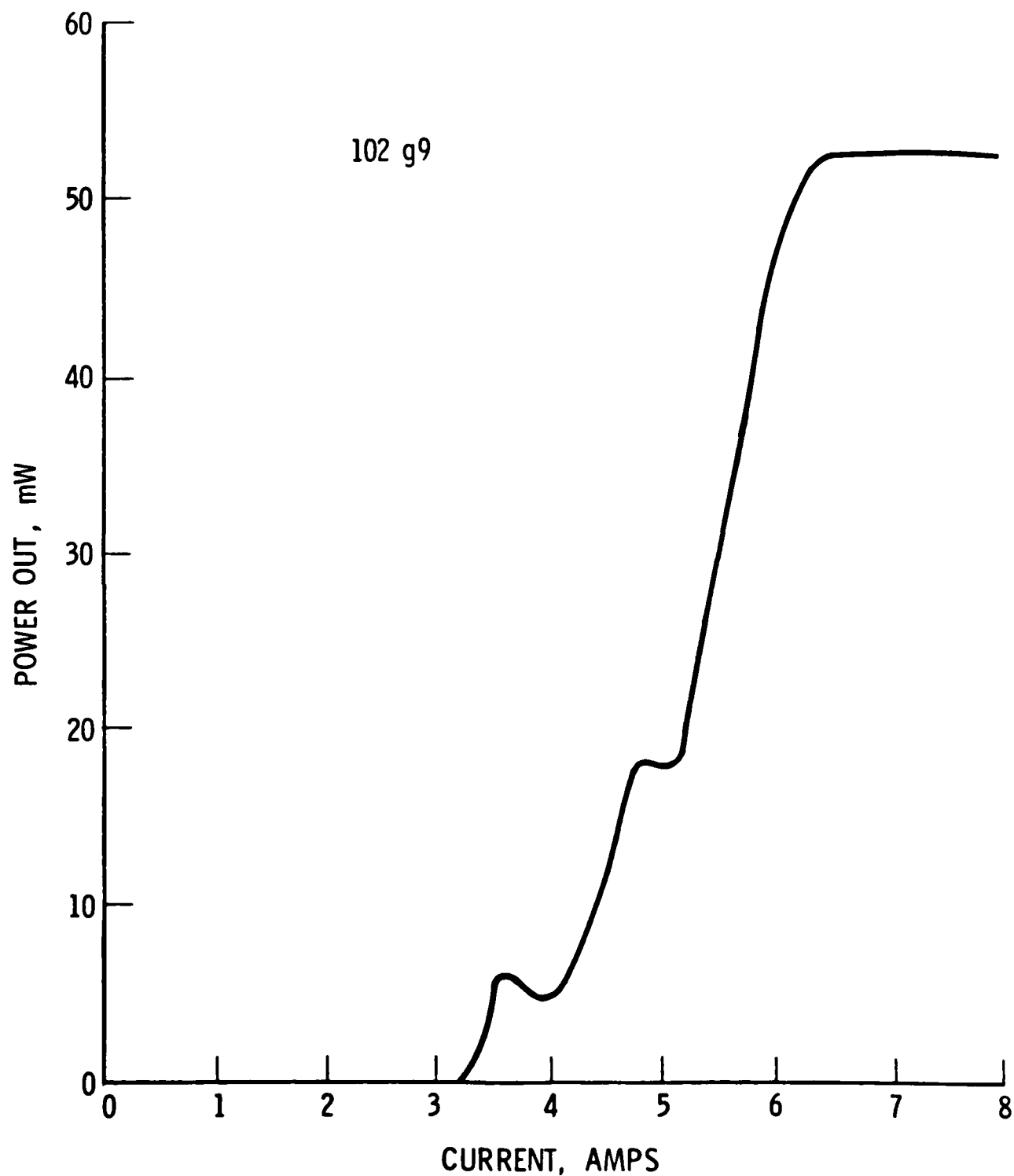


Figure 12 Total light power out as a function of total current to the diode.

Since kinks seem to be related to the filamentary structure of lasers, and since we were interest in beam quality in order to perform beam expansion, we made a careful study of the diffraction qualities of the light emitted from the DBR lasers. Depending on the device, we were able to observe diffraction limited operation, just above threshold. This is demonstrated by studying the divergence of sample g9, right above threshold. Near field patterns were observed both out the cleave and the grating face (Fig. 13). In addition, the in-plane beam divergence was measured coming out of the cleave. This was done by monitoring the spot size as a function of distance from the cleave. The data are shown in Fig. 14.

The data are analyzed by comparing the measured divergence with that expected for a Gaussian beam of the width determined from the near field intensity profiles (Fig. 13). The angular divergence of a Gaussian beam is given by

$$\theta_0 = \lambda/\pi w_0$$

where  $\theta_0$  is the half-angle and  $w_0$  is the half width of the beam at  $1/e^2$  in intensity.

Redefining the quantities in terms of full width half maximum,

$$\theta = \frac{\lambda}{0.72\pi\omega} .$$

The filament measured in the near field had an apparent width of 6.4  $\mu\text{m}$  (correction has not been made for resolution of the microscope objective used in this measurement). The far field beam divergence out the cleave was 0.072 rad, which corresponds to the diffraction expected from a filament of width 5.4  $\mu\text{m}$ . This is in good agreement with the measured filament width, and supports the assumption that this laser operated in a single spatial mode.

The laser output from the grating face was observed to have a near field profile which was a single filament 22  $\mu\text{m}$  wide. This profile is the beam which has diffracted from the 5.4  $\mu\text{m}$  filament in the laser region due to the use of a 1  $\text{mm}$  long grating as shown in Fig. 15. If the filament is assumed to extend the length of the active region of the laser diode, and begins to

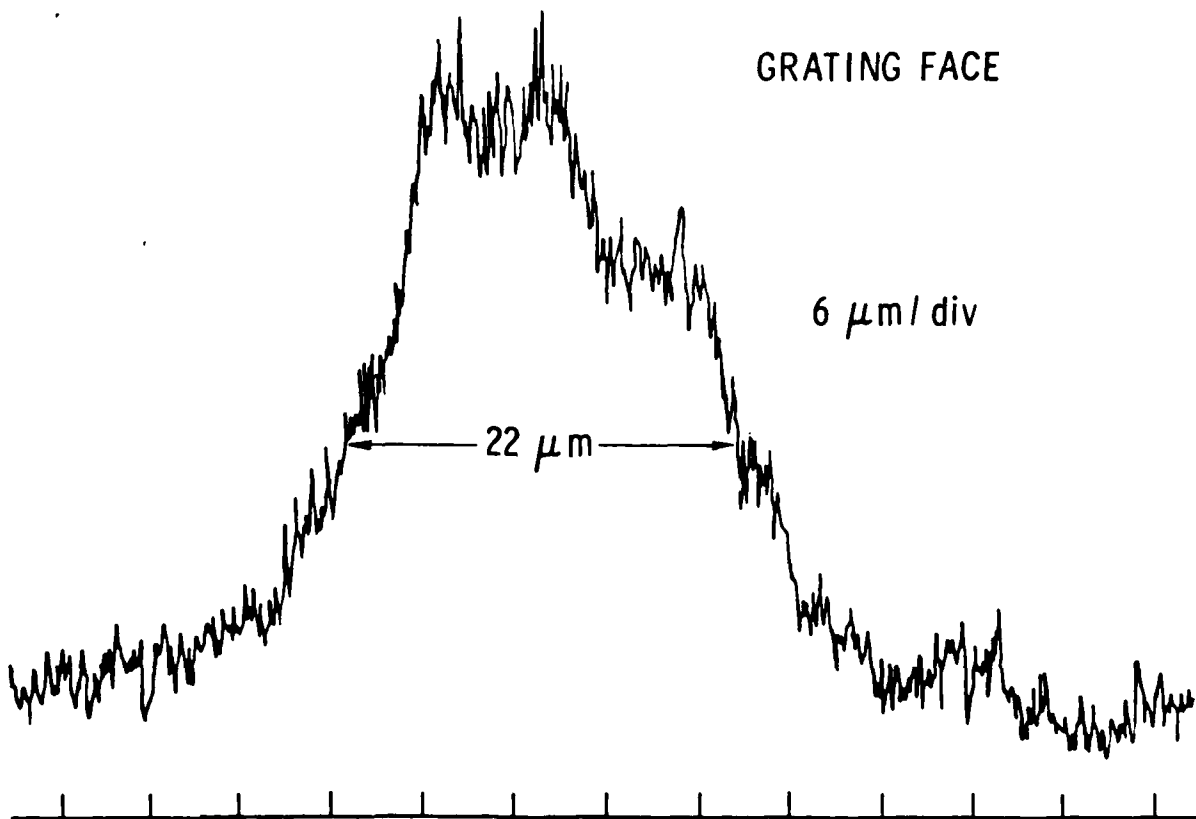
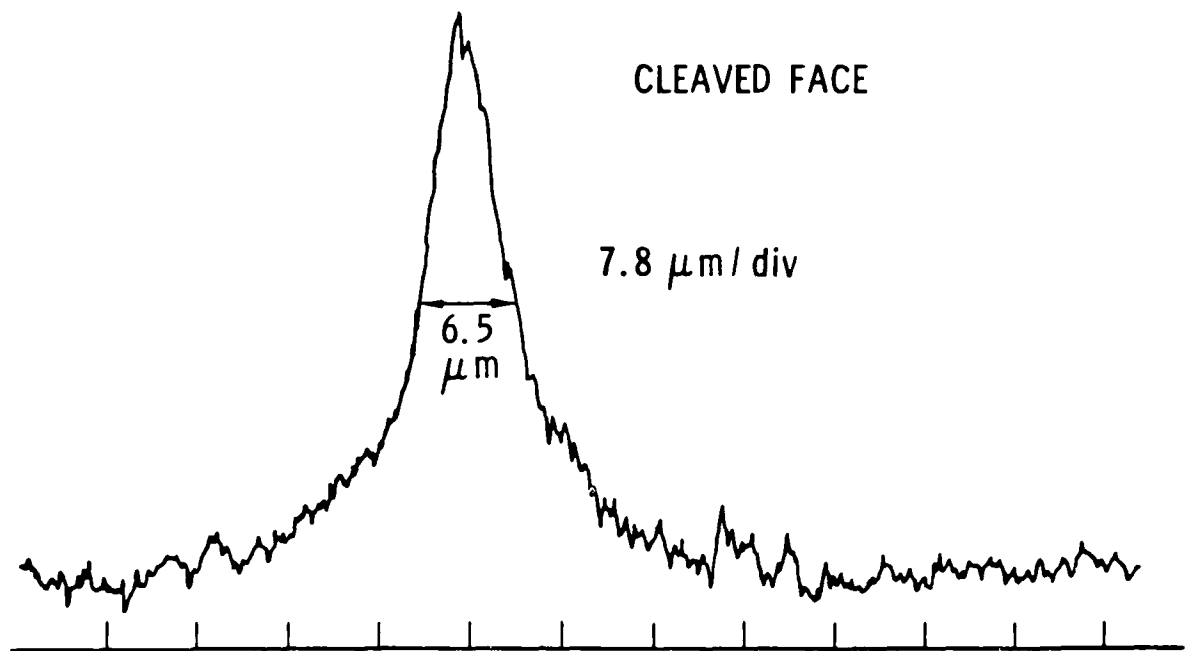


Figure 13 Diffraction-limited near-field patterns for the DBR laser output from diode g 9 just above threshold.

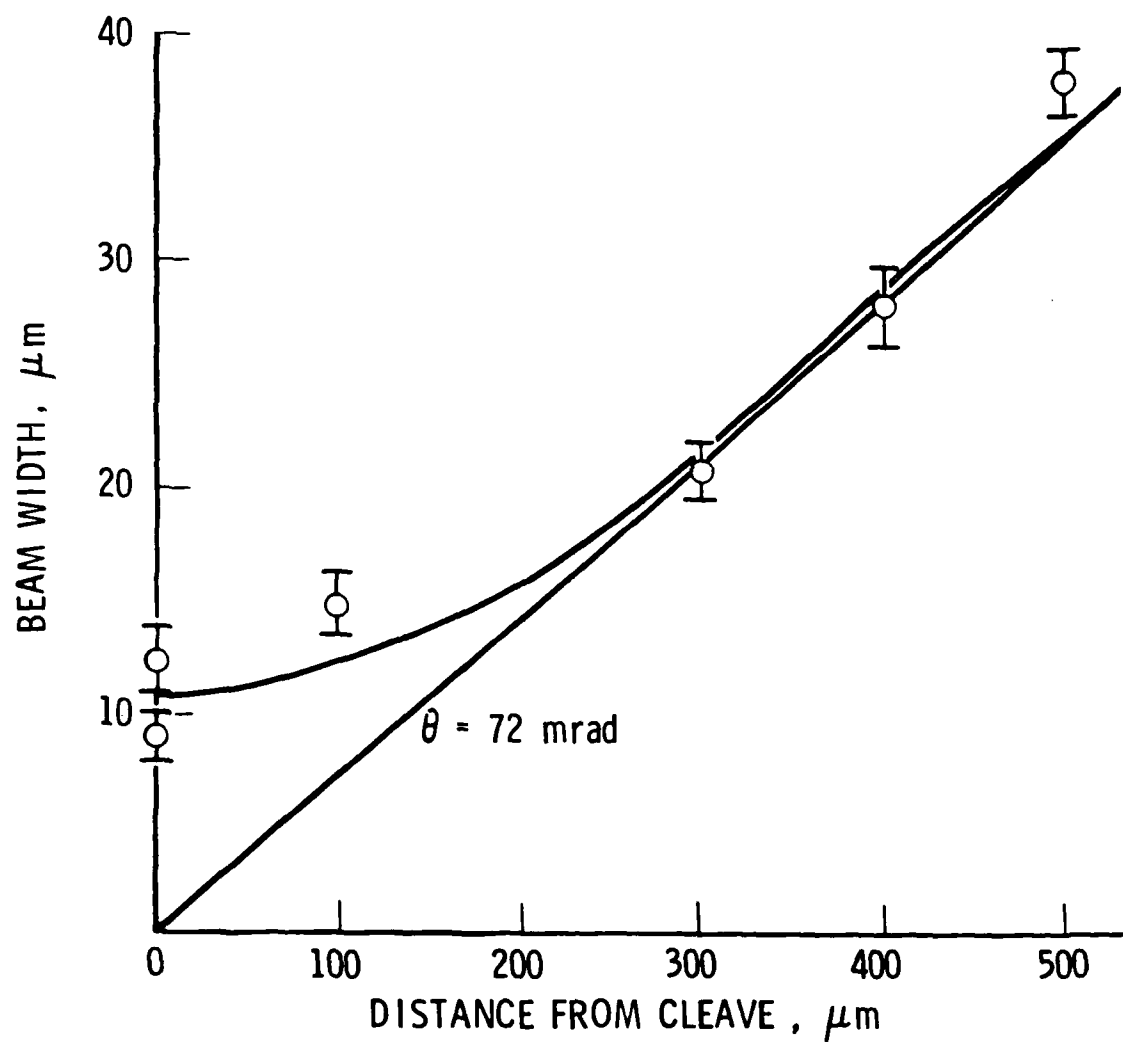


Figure 14 In-plane beam width as a function of distance from the exit face (as measured on a television monitor). Far field divergence angle is 72 m rad.

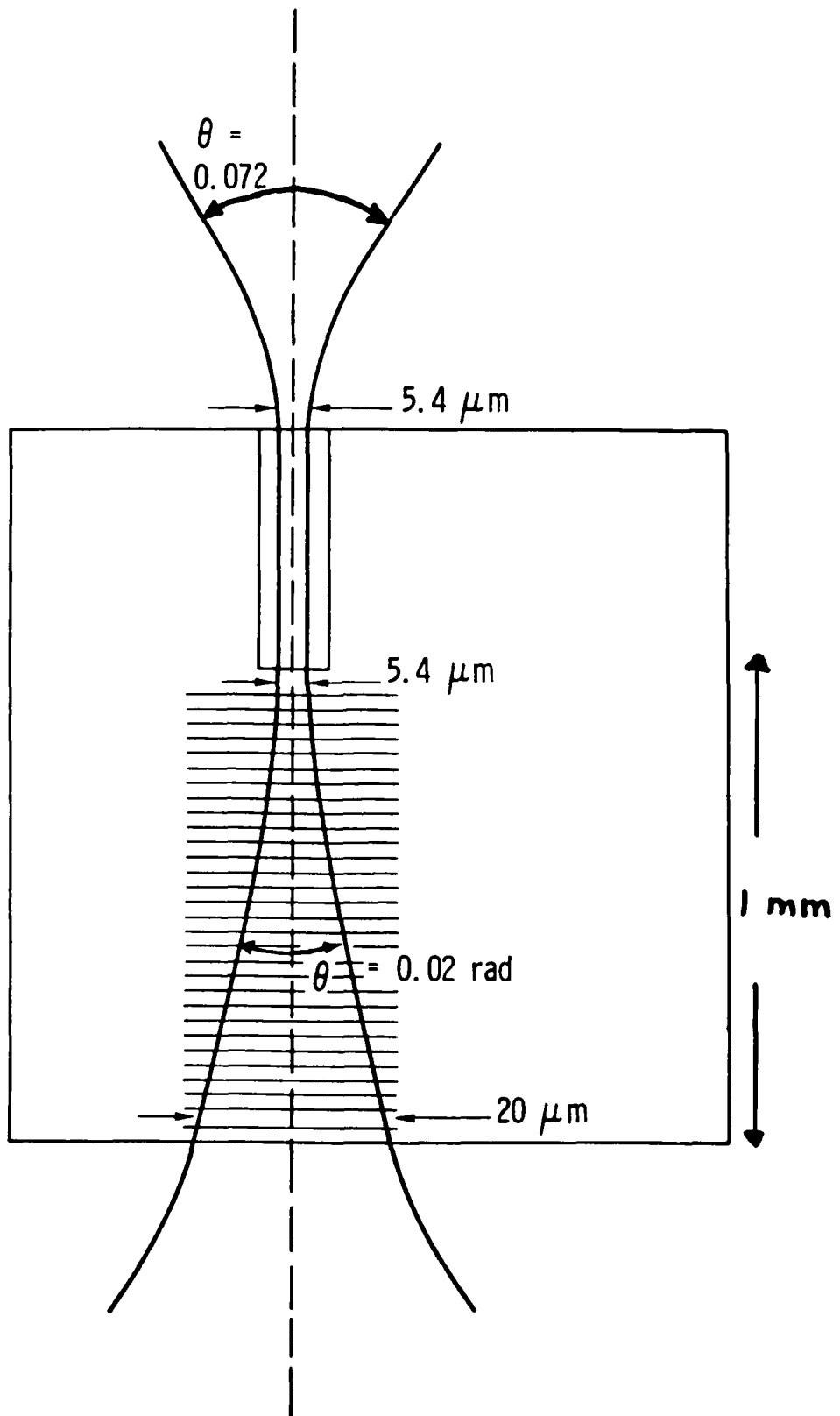


Figure 15 Diagram of top view of DBR laser, showing diffraction limited behavior of diode g 9.

expand when it enters the grating, then the diffraction should occur for a distance of 1 mm, at an angle given by the far field divergence angle divided by the index of refraction of the medium (0.02 rad). This divergence would cause the output of the grating to have a width of 20  $\mu\text{m}$ . This compares favorably with the measured filament width of 22  $\mu\text{m}$ .

For completeness, out-of-plane beam divergence was measured also. It was observed that the frequency corresponding to the higher order waveguide mode caused a double-humped far field pattern from the cleave. The divergence was greater than 0.48 rad and could not be measured since it was limited by the aperture of the lens which was used. The other frequency was a lowest order waveguide mode and had a beam divergence of 0.3 rad. This proves the assumption discussed earlier that the two frequencies are due to different modes occurring in the laser region.

Other diodes did not necessarily show in-plane diffraction limited behavior. The near field profiles of diode g5 are shown in Fig. 16. Although the apparent near field profile was 15  $\mu\text{m}$  wide, the beam divergence was 0.16 rad, corresponding to a filament size of 2.4  $\mu\text{m}$ . In other words, the diode had a highly filamentary character which caused a great deal of beam divergence. This fact was made clear by looking at the profile out of the grating. The output had several filaments and an overall width of almost 100  $\mu\text{m}$ . Diodes such as this would not be very useful for signal processing applications because of large beam divergence.

The result of this study is the fact that although DBR lasers control the longitudinal modes, they do not improve the spatial modes or ensure diffraction limited operation. It is necessary to control the spatial modes in order to obtain diffraction limited guided beams which can be expanded and used for coupling to fiber optics and for signal processing. The spatial control must be obtained by the same techniques used in producing single mode Fabry-Perot lasers: narrow stripes, tapered junctions, and other modes control devices.

### III. WAVEGUIDE BEAM EXPANSION

Beam expansion is achieved by using a distributed Bragg deflector (DBD). This device consists of a corrugated waveguide, whose grating is slanted at an angle  $\theta$  with respect to the incident beam. The geometry of the

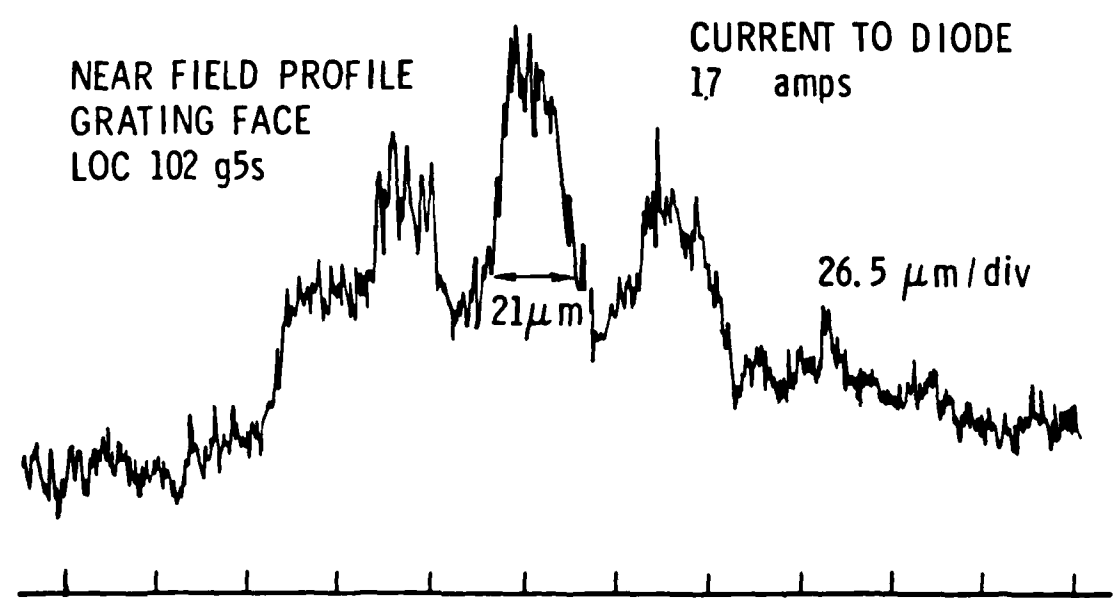
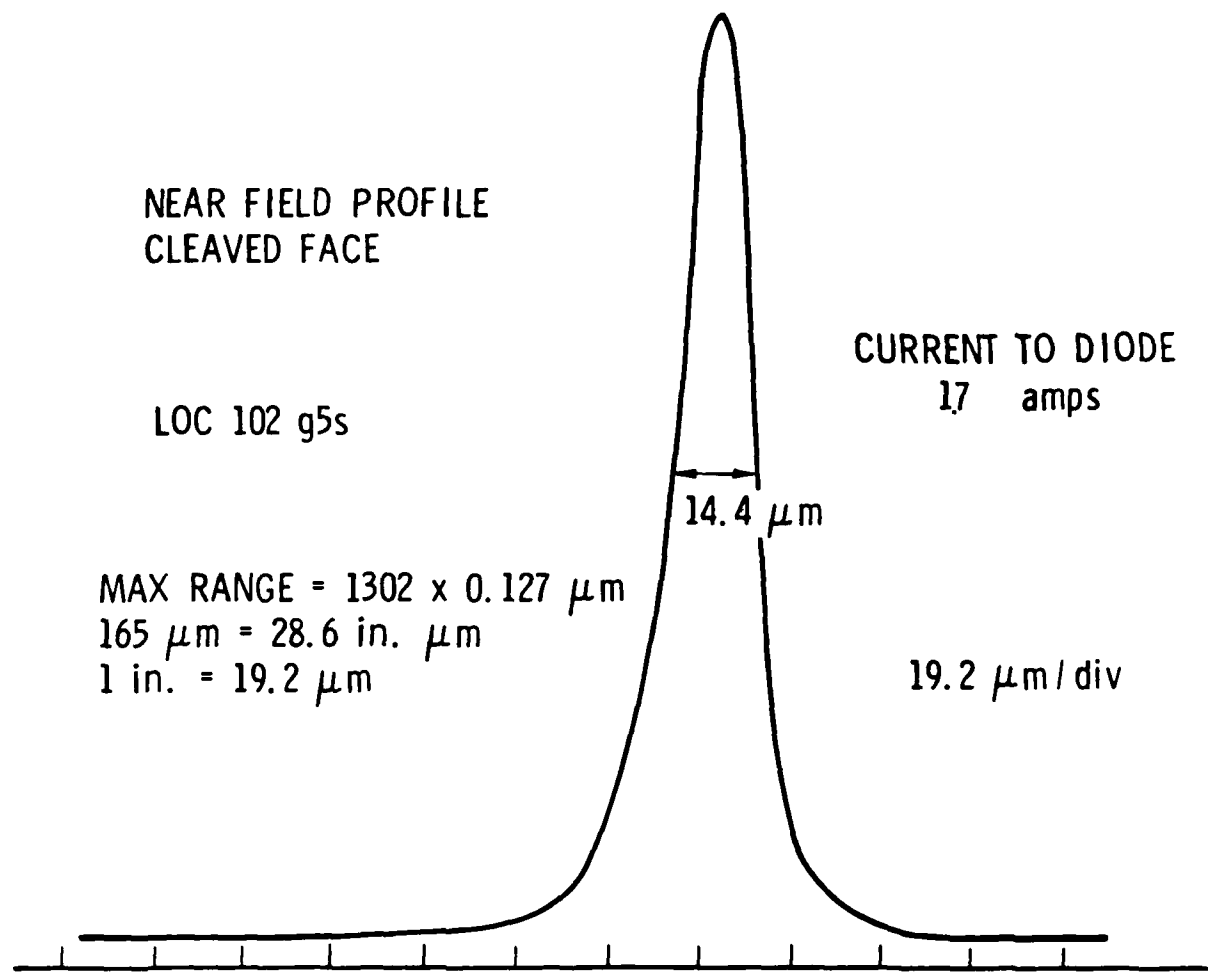


Figure 16 Near field profiles of diode g 5, demonstrating non-diffraction-limited behavior, even right at threshold.

DBD is shown in Fig. 17. The incident beam enters from the left into a confined slab guide with a corrugated surface. Bragg reflection occurs from the grating, reflecting the beam at an angle equal to the incidence angle so that the total deflection angle  $\theta_B = 2\theta$ . However, the reflections from the corrugations add up coherently only if the Bragg condition is satisfied; that is,

$$\Lambda = \frac{\lambda m}{2n \sin \theta}. \quad (8)$$

In addition to beam expansion, applications of the DBD include beam splitters (power division), deflectors (as, for example, to create ring geometries), polarizers and analyzers (with  $90^\circ$  deflection) and multiplexers/demultiplexers (with chirped gratings).

The theoretical analysis of the device has already been published.<sup>(2)</sup> It was found that the incident light beam amplitude is reduced while travelling through the DBD region by an exponential factor with distance,  $\exp(-\gamma z)$ , due to deflection. The results of the calculation are:

$$\gamma_{TE} = v \cos^2 \theta_B \quad (9)$$

and

$$\gamma_{TM} = v \frac{2 n_2^2}{(n_2^2 - n_1^2)} \log \left( \frac{n_2}{n_1} \right) [\cos \theta_B - 1] - \cos \theta_B^2, \quad (10)$$

where

$$v = w \frac{4\pi (n_2^2 - n_1^2) d^3}{3 (2\ell - 1) n_2 \lambda_0 t_e^3} \quad (11)$$

The quantities are as defined in Fig. 17, with  $\lambda_0$  the wavelength of incident light,  $\ell$  the Bragg scattering order and  $t_e$ , the effective guide thickness. If the mode is near cutoff,  $t_e = t + 1/\delta$ , where  $\delta$  is the exponential decay profile of the mode in the substrate.

Consider the deflection of a TM polarized beam at  $90^\circ$ , which is the configuration of greatest interest for beam expander applications:

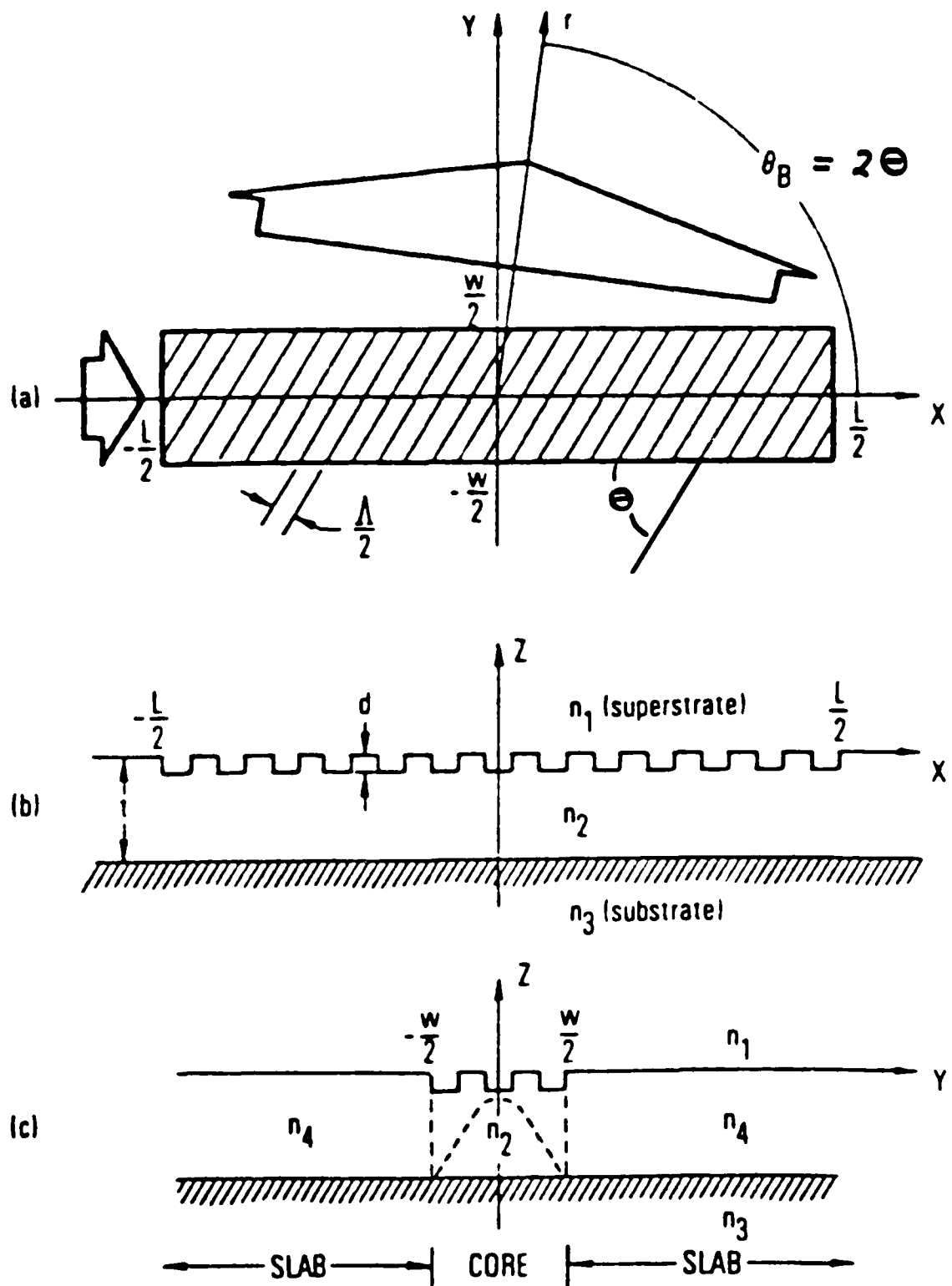


Figure 17 Distributed Bragg deflector: (a) top view; (b) side cross-sectional view; and (c) end cross-sectional view. Small and large (solid) arrows in (a) represent incident and deflected beams respectively. Dashed sinusoid in (c) represents equivalent core field distribution in the  $y$  direction.

$$\gamma_1 = v \frac{2 n_2^2}{\frac{n_2^2}{n_2^2 - 1} \log n_2} \quad (12)$$

We have made use of the fact that  $n_1 = \text{air} = 1$ .

It is convenient to relate these results to those of retroreflection in a corrugated waveguide, given in Eq. 4. Plugging the expression for the coupling coefficient into the expression for  $v$ , we write the DBD exponential coefficient as

$$\gamma_1 = \frac{4 n_g^2 \log n_g}{\pi (n_g^2 - 1)} K_w^2 \quad (13)$$

Since the deflected beam has an amplitude which decreases with distance along the DBD according to an exponential with a coefficient  $\gamma$ , the intensity width of the expanded beam will be approximately  $1/2\gamma$ .

Defining the expansion factor as the width of the deflected beam divided by the incident beam width, we write the expansion factor as

$$F_1 = \frac{1}{2\gamma_1 w} = 2 \frac{\pi (n_g^2 - 1)}{4 n_g^2 \log n_g} \frac{L_g^2}{w^2} \quad (14)$$

$$\equiv 2f^2 \left( \frac{L_g}{w} \right)^2$$

where we have defined the grating by its characteristic length,  $L_g$

It can be seen that it is easy to obtain large expansion factors, since the characteristic length of gratings can be typically larger than  $w$ . Large expansion factors are of interest for the application described in Figure 2, the low beam divergence laser. In this case, it is of interest to obtain expansion factors of roughly 100, to expand the  $10 \mu\text{m}$  emission from a GaAs stripe geometry laser to  $1000 \mu\text{m}$  beam, which could be used with an output grating coupler to make the HBL. For the case of GaAs waveguides,  $n_g = 3.6$ , and  $f = 0.56$ . Thus expansion of a factor of 100 can be achieved if  $L_g/w = 13$ . For an incident beam of  $10 \mu\text{m}$ , this requires  $L_g = 130 \mu\text{m}$ , or  $K = .004$ . Gratings with this coupling coefficient were achieved in the DBR lasers. Thus we expect the beam expander to produce the appropriate amount of expansion.

The research program was designed first to demonstrate beam expansion in high optical quality VPE GaAs waveguide material and then to apply the concept to LPE GaAs double heterostructures, so that the laser and beam expander could be combined into the same substrate.

Demonstration of beam expansion in VPE GaAs epilayers was successful. A perspective view of the Bragg-effect polarizer/analyizer which we fabricated is shown in Fig. 18. The asymmetric slab waveguide structure consisted of a  $1 \mu\text{m}$  thick, n-type ( $\sim 10^{16} \text{ cm}^{-3}$ ) GaAs layer epitaxially grown over a heavily doped n-type ( $\sim 5 \times 10^{18} \text{ cm}^{-3}$ ) GaAs substrate; it supported only the lowest order one-dimensional, T.E. - and T.M. - polarized modes. Ninety degree Bragg scattering of the incident  $1.15 \mu\text{m}$  radiation was accomplished via a second order periodic surface corrugation ( $\Lambda = 0.478 \mu\text{m}$ ) which was ion milled into the waveguide surface and overcoated with a  $0.1 \mu\text{m}$  thick layer of aluminum ( $n_1^2 \approx 69$ ) in order to increase its deflection efficiency. As revealed by SEM examination of a cross section through the device, the corrugations bore a nearly triangular tooth profile. A photograph of a typical grating is shown in Fig. 19. The total corrugation length,  $L$ , and input beam width,  $w$ , were  $3.2 \text{ mm}$  and  $50 \mu\text{m}$ , respectively.

Figure 20 shows a semi-logarithmic plot of the near-field, deflected beam intensity profile of one of our  $90^\circ$  Bragg deflectors. The data shows that the deflected beam decreases a factor of  $1/e$  in  $1.3 \text{ mm}$  length. With an input beam of  $50 \mu\text{m}$ , this corresponds to an expansion factor of 38. From this data it can be inferred that the effective coupling length of the grating was  $L_g = 385 \mu\text{m}$ , with a coupling coefficient of  $K = 0.0013$ . This coupling is too weak for the HBL. The reason for the weak effect is use of VPE GaAs. The index change due to the reduction of the number of free carriers in the epilayer is very small. As a result, the guided mode extends into the substrate and the effective guide width is much larger than the  $1 \mu\text{m}$  physical thickness of the epilayer. For the physical parameters used in the experiment, the effective guide thickness was several microns, causing the coupling coefficient to be small.

Because of the weakness of guiding in the VPE material, the effective waveguide thickness was large and the grating coupling coefficient was small. As a result, the expanded beam was too large to be useful for more than demonstration of the principles. However, it was demonstrated that even a grating with a low coupling coefficient can be used successfully as a

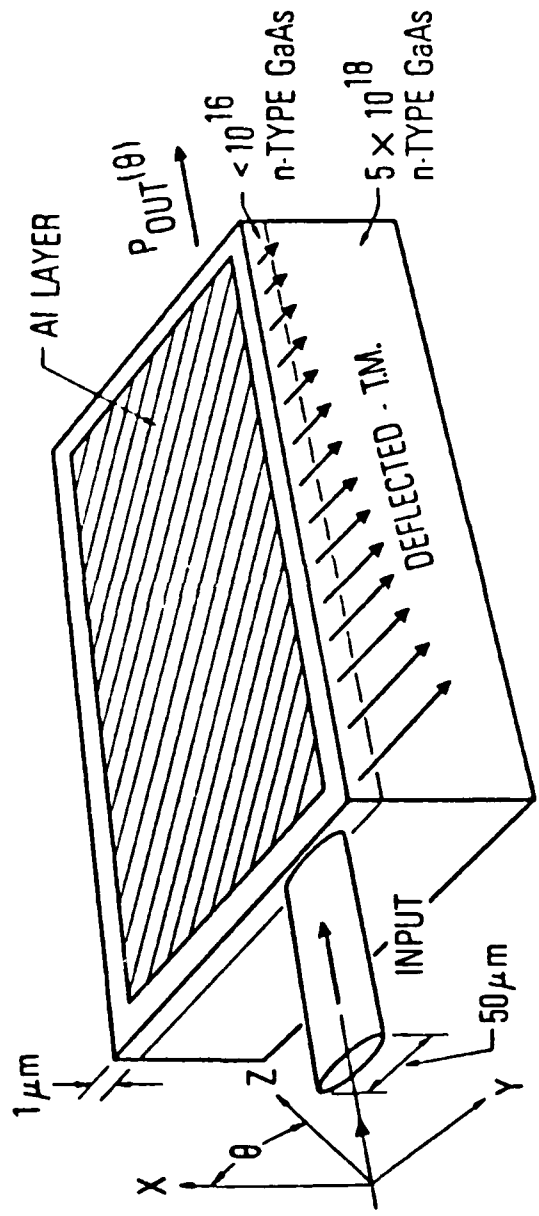


Figure 18 Perspective view of the Bragg-effect polarizer/analyser which was tested. The electric field vector of the input beam is oriented at an angle  $\theta$  to the waveguide surface normal.

## Ion Milled Grating



$0.5 \mu\text{m}$  PERIOD

Figure 19 Typical grating fabricated by ion milling through a photolithographically prepared photoresist mask

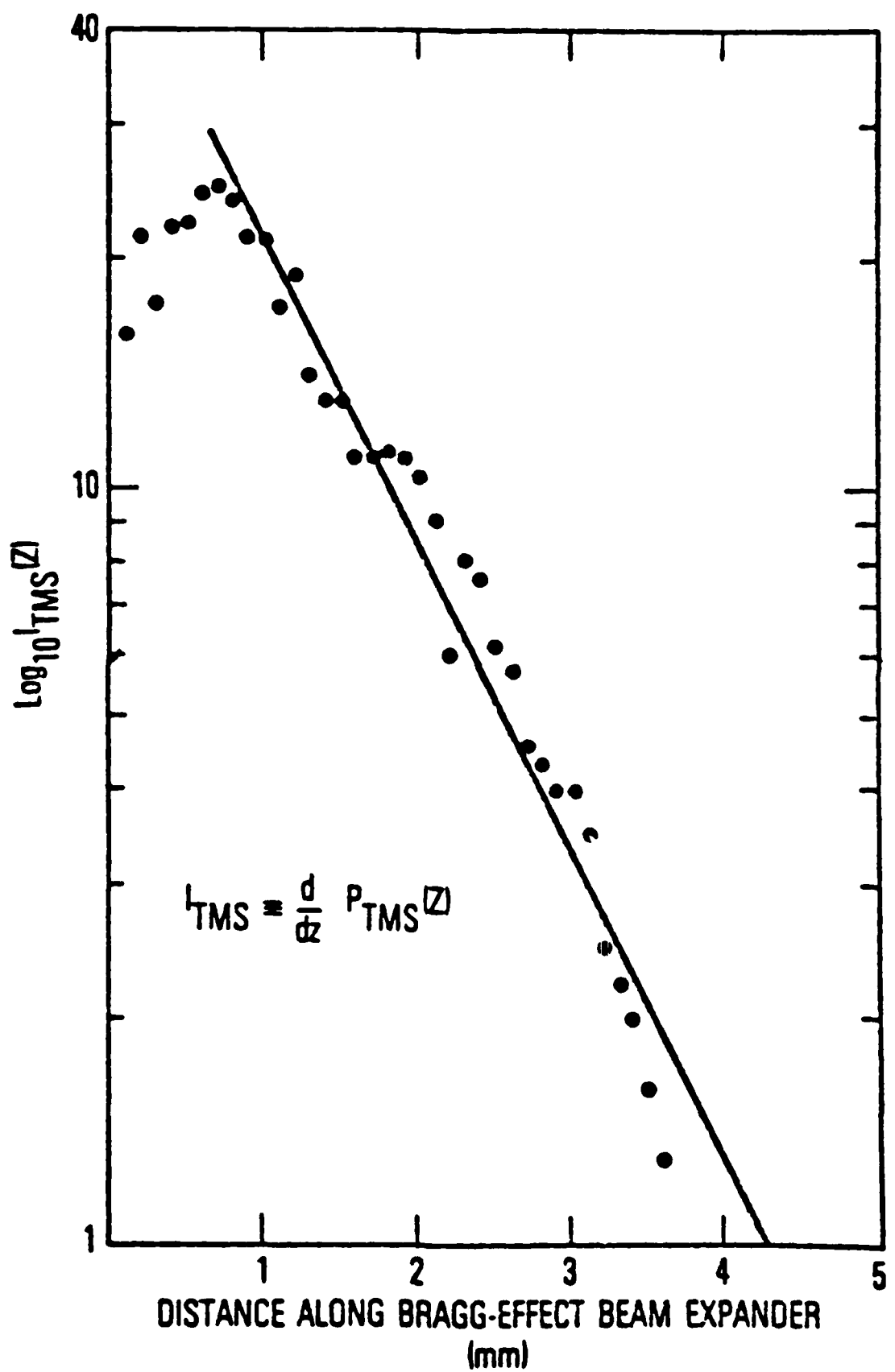


Figure 20 Semi-logarithmic plot of the near-field Bragg-scattered beam intensity profile of a 90° deflector.

polarizer-analyzer. (3)

Operation of the DBD as a polarizer/analyizer can be seen by observing that  $\gamma_{TE} = 0$  for a deflection angle of  $90^\circ$ . Polarizer/analyizer performance parameters of interest include the extinction ratio,  $\rho$ , which we define as being equal to the ratio of T.M. - to T.E. -mode power deflected by the device, or

$$\rho = \frac{\gamma_{TM}}{\gamma_{TE}} \cdot \frac{\delta_{TE}}{\delta_{TM}} \cdot \frac{1 - \exp(-2 \delta_{TM} L)}{1 - \exp(-2 \delta_{TE} L)}, \quad (16)$$

and the T.M. deflection efficiency,  $\eta$ , which we define as being equal to the ratio of deflected to incident T.M. -mode power, or

$$\eta = \frac{\gamma_{TM}}{\delta_{TM}} [1 - \exp(-2 \delta_{TM} L)]. \quad (17)$$

In Eqs.(16) and (17),  $\delta_{TE}$  and  $\delta_{TM}$  are the total (including background) T.E. - and T.M. -mode attenuation coefficients, respectively, and  $L$  is the device length.

Experiments were performed on the polarization dependence of beam deflection using the VPE GaAs waveguide beam expander shown in Fig. 18. By measuring the near field intensity profile of the beam which was Bragg deflected by the polarizer/analyizer,  $\delta_{TM}$  was determined to be  $4.19 \text{ cm}^{-1}$ . Knowledge of  $\delta_{TM}$  together with measurements of the undeflected throughput power,

$$P_{out}(\theta) = P_{in} [\cos^2 \theta \exp(-2 \delta_{TM} L) + \sin^2 \theta \exp(-2 \delta_{TE} L)] \quad (18)$$

for  $\theta = 0$  and  $\pi/2$ , were then used to yield  $\delta_{TE} = 3.11 \text{ cm}^{-1}$ ,  $\gamma_{TM} = 0.154 \text{ cm}^{-1}$ , and  $\eta = 0.034$ . Finally, direct measurement yielded an extinction ratio of 343 from which it was inferred that  $\delta_{TE} = 3.6 \times 10^{-4} \text{ cm}^{-1}$ . Figure 21, which plots  $P_{out}(\theta)$ ,  $P_{TMS}(\theta)$  (the total T.M. power deflected), and the experimental data, summarizes the results.

The passive beam expander in VPE GaAs demonstrated that beam expansion was indeed possible using the Distributed Bragg Deflector. However, it was

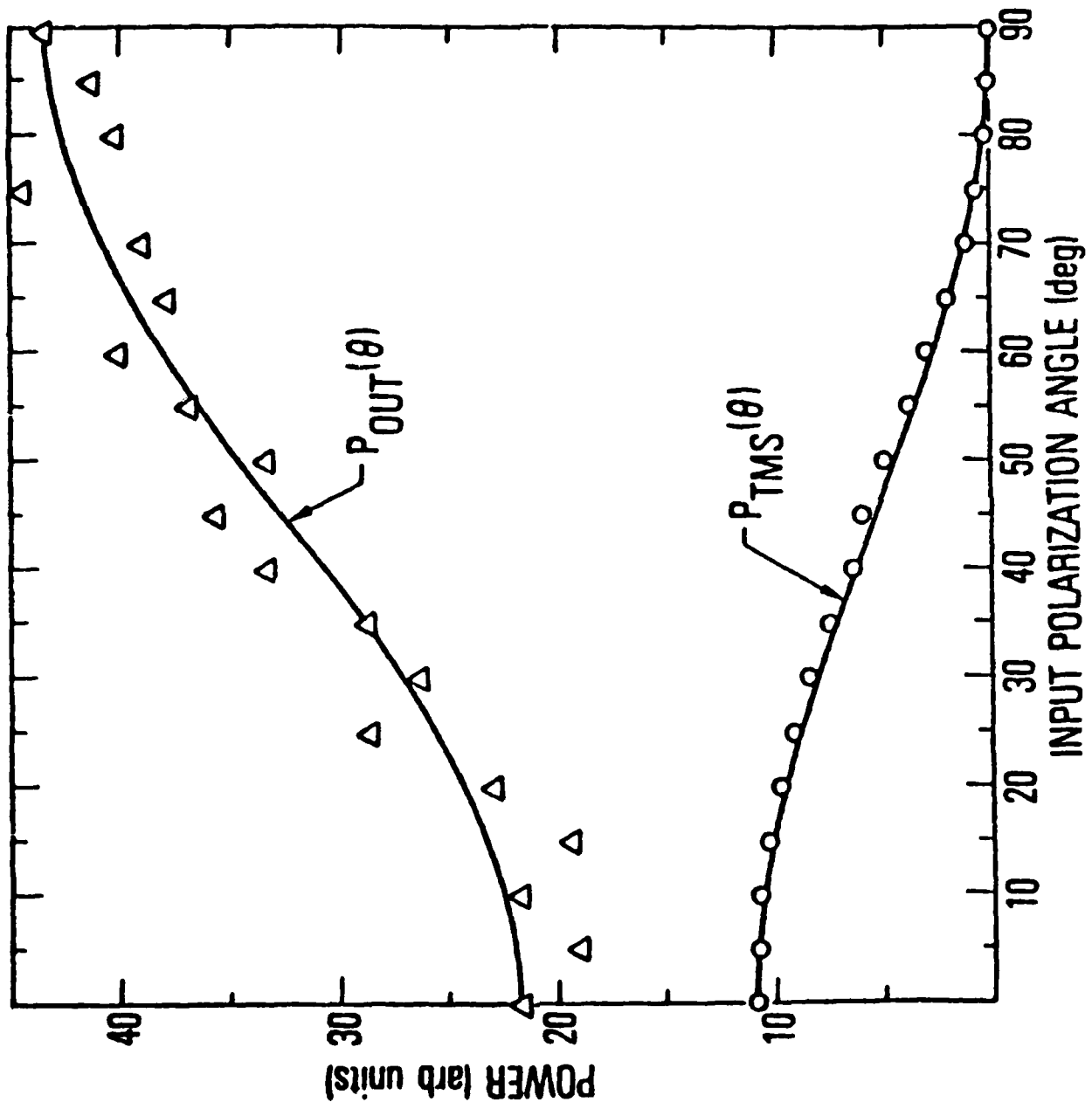


Figure 21 Plots of the throughput power,  $P_{\text{OUT}}(\theta)$ , and Bragg-scattered power,  $P_{\text{TMS}}(\theta)$  as functions of the input beam polarization angle  $\theta$ . Also shown are the experimental data ( $\Delta$  and  $\circ$ ).

also demonstrated that the efficiency of deflection goes to zero for the TE mode at a deflection angle of  $90^\circ$ . This means that the  $90^\circ$  angle of deflection is not suitable for use in a monolithic circuit together with a DBR laser source. Since the DBR lasers we fabricated were found to operate with a TE polarization, no deflection will occur at  $90^\circ$ . This means that the angle of deflection must be some angle other than  $90^\circ$ . The most convenient angle of deflection is  $45^\circ$ .

Figure 22 shows a  $45^\circ$  DBD which was fabricated in VPE GaAs. The beam expansion is shown in the lower photograph, as a streak to the left of the beam. The difficulty in observing this device is the necessity of polishing the end face to obtain the output at  $45^\circ$ . The advantage is that the grating can be used in fundamental order. The deflection of the DBD in the VPE waveguide was very weak because the waveguide was so thick. Experiments on  $45^\circ$  deflection in thinner LPE GaAs waveguides await integration with DBR lasers.

It is possible to use the results of the DBR lasers and the coupling coefficients of their gratings to predict the behavior for the  $45^\circ$  beam expander. The  $45^\circ$  beam expander used in conjunction with a GaAs DBR laser will be used with the grating in fundamental order and a spacing of  $0.338 \mu\text{m}$ . To determine the expansion factor from the  $K$  value of the grating, we use Eq. (9) and obtain  $\gamma_{TE} = (2K/\pi)^2 w \cos^2 \theta_B = w \cos^2 \theta_B / (\pi L_g)^2$ . We wish to determine whether or not teeth of the shape used for the DBR laser can be satisfactory to produce beam expansion of the requisite factor of 100. First we need to define an expansion factor, which includes the fact that the deflection is at an angle other than at  $90^\circ$ . The width of the expanded beam is  $\sin \theta_B / (2 \gamma_{TE})$ . This gives an expansion factor of

$$F_\theta = \frac{1}{2} \left( \frac{\pi L_g}{w} \right)^2 \frac{\sin \theta_B}{\cos^2 \theta_B}. \quad (19)$$

The expansion factor increases rapidly as  $\theta \rightarrow 90^\circ$ , but at this angle the TE reflectivity  $\rightarrow 0$ , so there is no inconsistency. When  $\theta = 45^\circ$ , the expansion factor will be

$$F_{45} = \left( \frac{\pi L_g}{w} \right)^2 / \sqrt{2}. \quad (20)$$

## 45° Beam Expander

NEAR FIELD IMAGE  
BEFORE AND AFTER ALIGNMENT

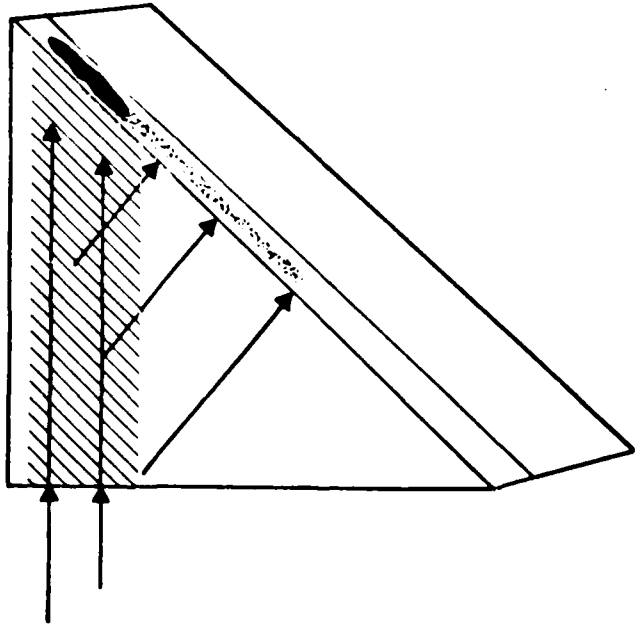
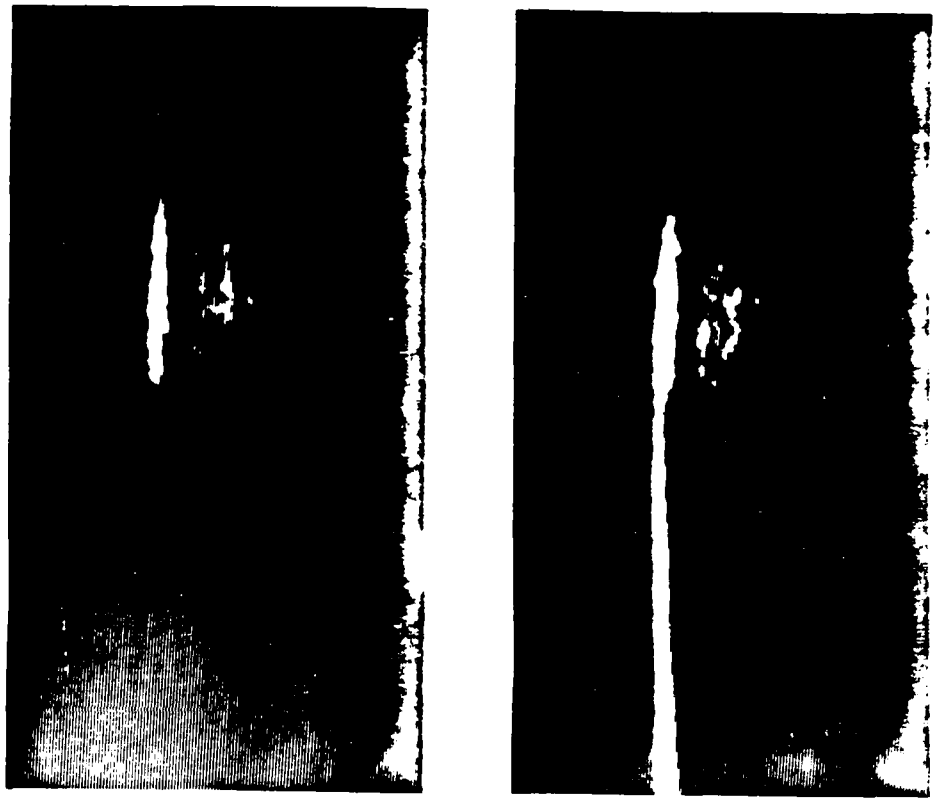


Figure 22 Geometry for 45° beam expander along with photographs of an IR television monitor of near field image of guided beam. The top photograph represents the unexpanded beam 50  $\mu\text{m}$  wide before proper angular alignment. The bottom photograph demonstrates beam expansion with the streak to the left.

The DBR lasers we fabricated had an average  $K = 0.0035$  and effective grating length  $L_g = 140 \mu\text{m}$ . From Eq. 4, it can be seen that the effective length of a grating used in first order differs from the effective length of a grating used in third order by a factor of 3. In first order these gratings would have  $L_g = 47 \mu\text{m}$ . From Eq. 20 it can be seen that for  $w \sim 10 \mu\text{m}$ , the  $45^\circ$  expansion factor will produce a beam which is 1.5 mm wide. Appropriate beam expansion will result from gratings such as those made for the DBR lasers. Proof requires fabrication of the  $45^\circ$  beam expander on double heterostructure material, a task we have delayed until we develop techniques to monolithically integrate the DBR laser with the beam expander.

#### REFERENCES

1. "Laser Oscillation in Epitaxial GaAs Waveguides with Corrugation Feedback", M. Nakamura, H. W. Yen, A. Yariv, E. Garmire, S. Somekh, H. L. Gavin, *Appl. Phys. Lett.* 23 244 (1973).
2. "Distributed Bragg Deflector: A Multifunctional Integrated Optical Device", H. M. Stoll, *Applied Optics* 17, 2562 (1978).
3. "Bragg-effect Polarizer/Analyzers and Lens-less Waveguide Beam Expansion", H. M. Stoll, W. E. Soady, *Proceedings of the Optical Society Topical Conference on Integrated Optics*, January 1980.

#### IV. NEW DESIGNS FOR THE HIGH BRIGHTNESS LASER

It was discovered in Chapters II and III that the DBR lasers prefer the TE polarization, while the beam expander does not deflect TE polarization at  $90^\circ$ . This makes it necessary to consider design changes, although we will show that design changes may not be necessary. These design changes require forcing the laser to operate in the TM polarization, so that the beam expander will work at  $90^\circ$ , or changing the angle of the beam expander, so that it will expand a TE-polarized laser beam.

The first design requires forcing the laser to operate in the TM polarization. This may be done by placing the retro-reflector after the beam expander, as shown in Fig. IV-1. In this design grating retro-reflector and grating output coupler have periodicities and blaze angles specially chosen to optimize their duties; the former to act as a mirror, the latter to couple out. The ability for a laser to operate with a beam expander inside the cavity is the risk factor in this device. The first experiments after demonstration of the DBR was an attempt to fabricate the laser design shown in Fig. IV-2, using a cleaved side of the diode as the second mirror, after the beam expansion. This was undertaken in order to test whether or not the design in Fig. IV-1 was viable. These diodes did not work. We assume the reason for the lack of success is the fact that the grating inside the laser cavity increased the loss, raising the threshold. Although this design is attractive because of the simple way in which many lasers may be locked (see Fig. 3, Chapter I) we are not very optimistic about its ultimate success until we reduce losses connected with waveguide and grating fabrication. Such designs will probably be more successful using epitaxial growth techniques such as metallo-organic chemical vapor deposition or molecular beam epitaxy.

The second design (Fig. IV-3) utilizes the beam expander at  $45^\circ$ , as described in Chapter III. This design has no inherent disadvantage over the original HBL design, except that an output coupler is required before it is possible to measure the effectiveness of the beam expander. This may require somewhat more elaborate studies leading toward monolithic integration than originally anticipated, but the design should operate with characteristics similar to the individual HBL originally proposed. The  $45^\circ$  beam expander may require somewhat more sophistication as to the locking of a laser array. Our

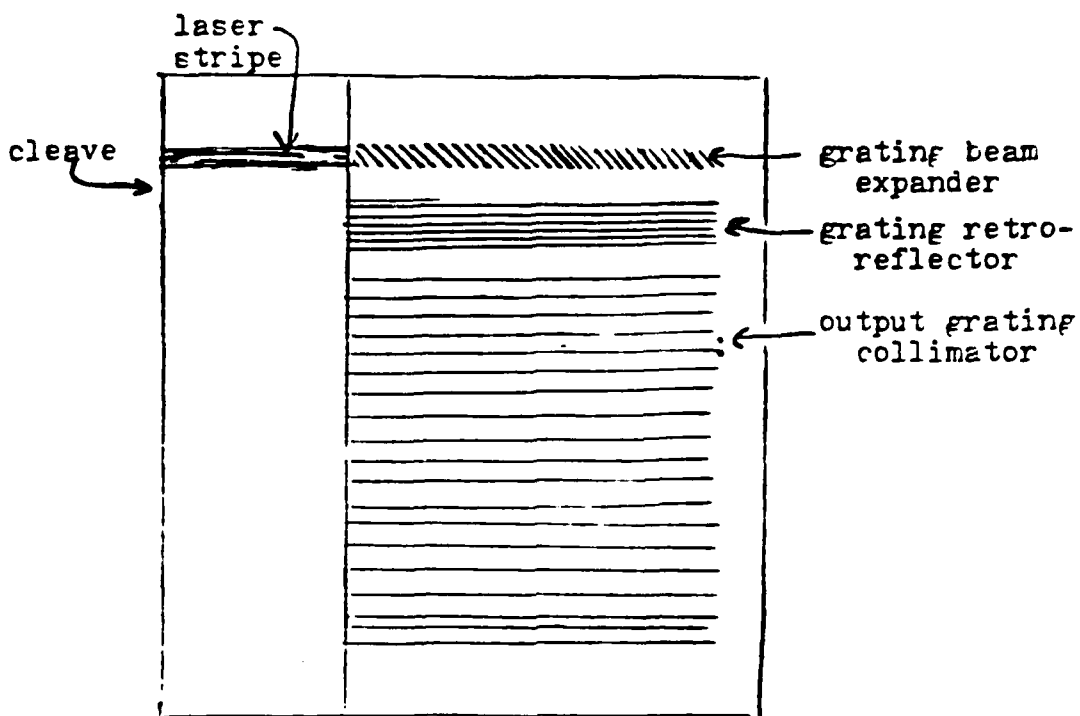


Figure IV-1. Design for high brightness laser in which retro-reflector is placed after 90° beam expander. This forces laser to operate in the TM polarization.

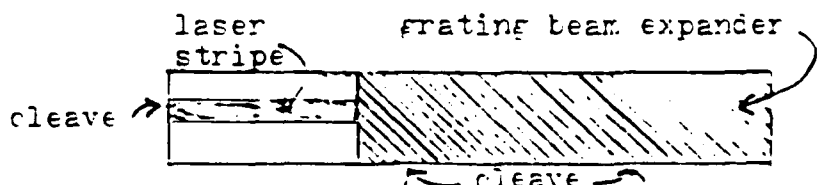


Figure IV-2. Design for first test device to determine whether lasers will operate with beam expander inside the laser cavity.

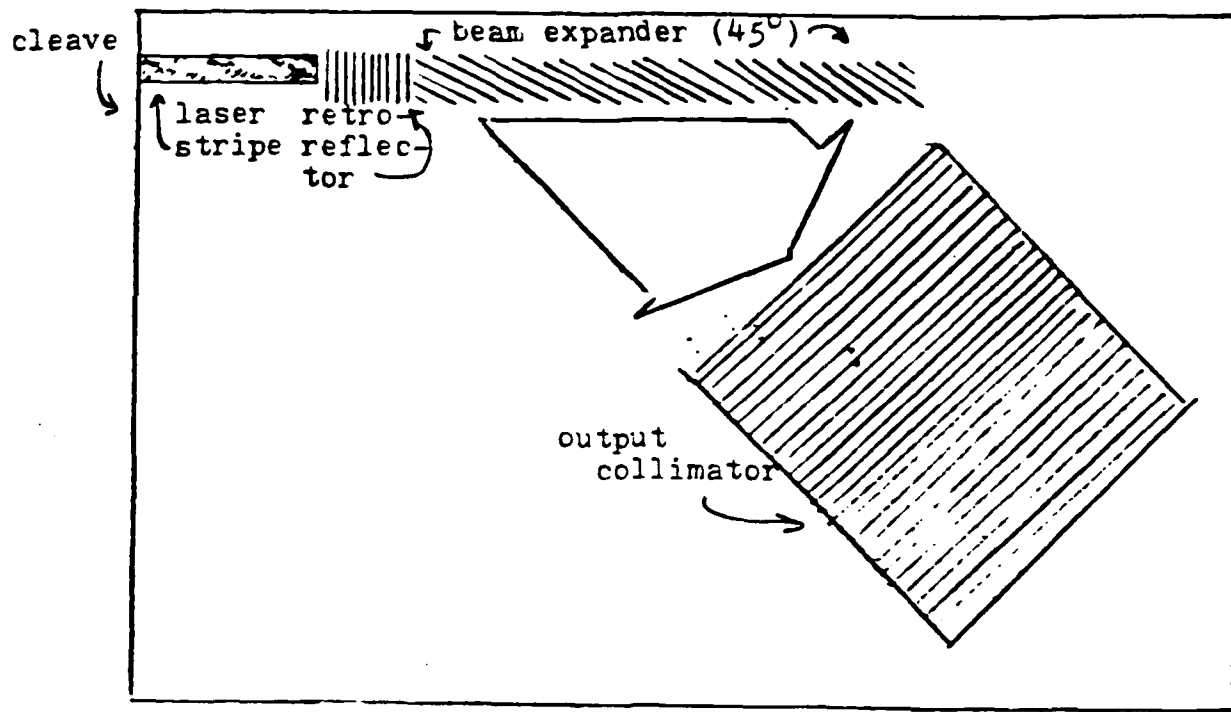


Figure IV-3. High brightness laser with  $45^{\circ}$  beam expander, operating on TE polarization, with output collimator grating oriented at  $45^{\circ}$  to the cleave.

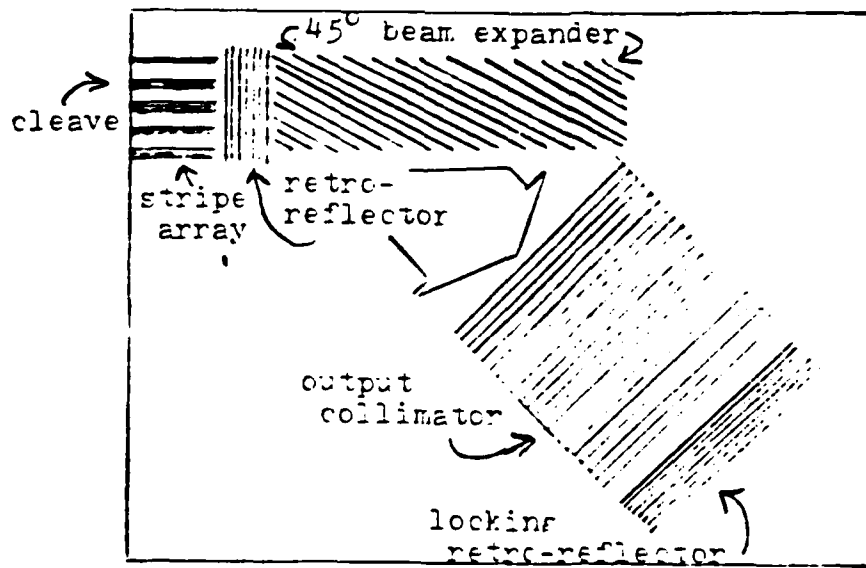


Figure IV-4. Locked high brightness laser array, using additional grating retro-reflector to phase lock the array

original proposal relied on a cleaved edge to retro-reflect after the output collimator and thereby lock the array. The use of the 45° beam expander means that there is no more cleaved edge for retro-reflection. One option is an additional retro-reflecting grating to replace the cleave, as shown in Fig. IV-4. However, there is another possible option. The grating spacing for the output collimator can be chosen so that the lowest order of the grating deflects and collimates the light out of the waveguide and into free space, while in higher order the grating retro-reflects. In fact, a grating which has a periodicity equal to the wavelength of the light in the medium acts as an output collimator in lowest order, while causes some retro-reflection in second order. A control of the amount of output coupling vs retro-reflection requires control of grating groove shape and blazing. The geometry shown in Fig. 4 (Chapter I) represents the design in which a single grating acts as output coupler and weak retro-reflector to ensure locking of modes.

The knowledge that the output grating also retro-reflects suggests the possibility that the design originally proposed (Fig. IV-5) may in fact work. The additional retro-reflection caused by the output coupler which would act with the beam expander on the TM mode may be sufficient to overcome the natural tendency of the DBR laser to operate TE polarized. The geometry of IV-5 may indeed operate TM polarized. It is difficult to obtain any theoretical information to confirm whether or not this latter design will work. It remains to be investigated experimentally.

The first experiments we shall undertake will be with design IV-3, as soon as the materials and fabrication problems are solved to the point where we can make DBR lasers reproducibly with reproducible properties. This is the portion of the research underway at the present time and described in the next chapter.

## V. MATERIALS AND FABRICATION STUDIES

The first successful DBR lasers were fabricated during Jan, Feb, and March, of 1979 by H. Stoll and his technician, W. Soady. There was one run, in which six successful diodes resulted. Extensive data on two of these diodes were taken at USC and were shown in Chapter II. These DBR lasers were fabricated from one epitaxial wafer purchased from Laser Diodes Laboratories. Out of the wafer that was received, most of the material was used

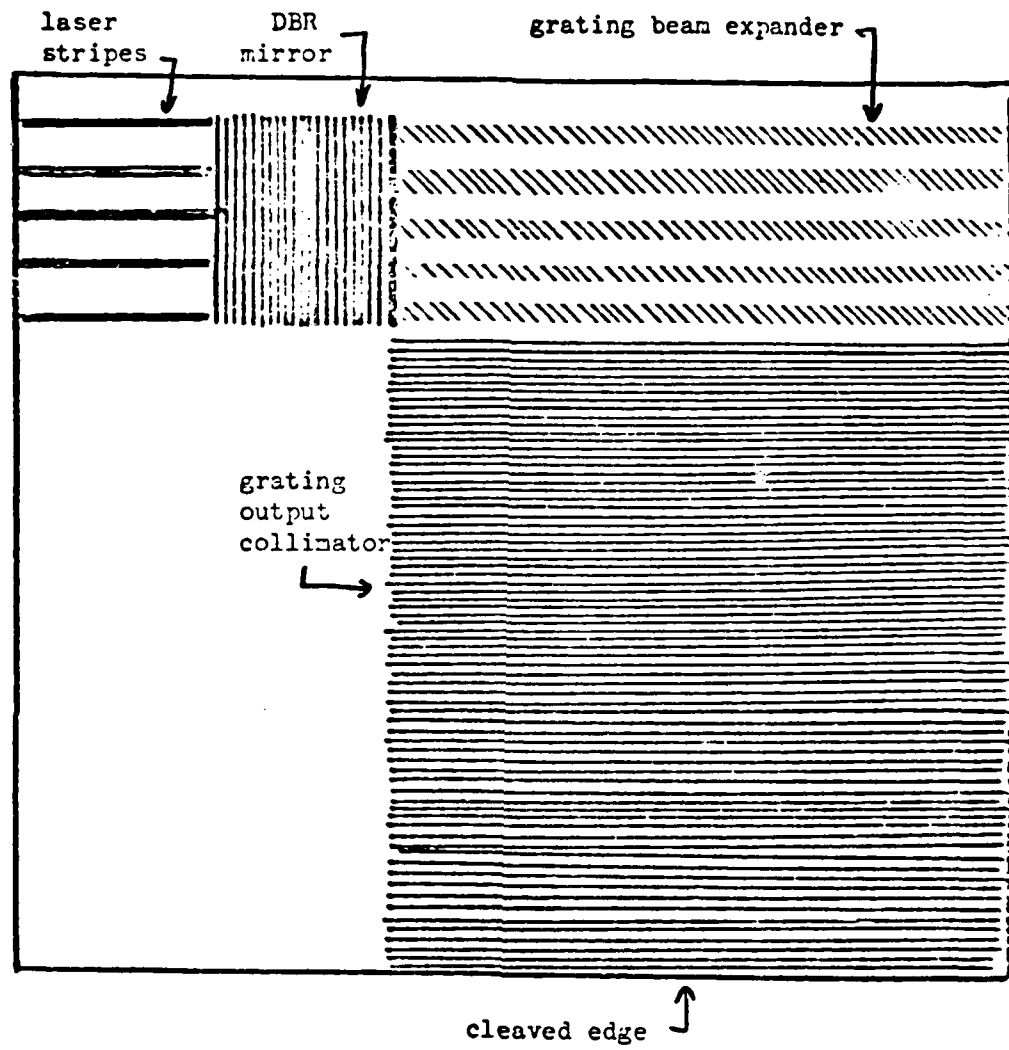


Figure IV-5. Three-mirror locked array, as originally proposed (includes two cleaved edges and DBR mirror)

in the preliminary testing and fabrication developments that lead to the successful DBR lasers. There remained one small piece of the same wafer. That piece was used up in an unsuccessful attempt to fabricate a laser of the design shown in Fig. IV-2.

Experiments were begun to fabricate DBR lasers on a new wafer from Laser Diode Laboratories and also on a wafer from Aerospace Corporation. We learned that a great deal of time had to be spent characterizing a given wafer before we knew enough information to proceed with fabrication of DBR lasers. These studies include angle lapping, IMMA and photoluminescence spectra. These data must be correlated to determine layer thicknesses and aluminum concentrations. In addition, planar and stripe geometry Fabry-Perot lasers must be fabricated to test laser thresholds.

Since it became apparent that it is important to get as much mileage out of a single wafer as possible, the Aerospace epitaxial growth facility expanded to use larger boats, designed to grow larger wafers. We expected that this would provide sufficient epitaxial material. Unfortunately, we discovered that the larger boat caused some unevenness on the waveguide layers which made them unsuitable for fabrication of DBR lasers. We therefore embarked on research to improve the flatness of our epitaxial layers, and to obtain better control on the aluminum concentration.

A second wafer was purchased from Laser Diodes Laboratories. After extensive photoluminescence and IMMA tests, it became apparent that the wafer from Laser Diode Laboratories had the wrong aluminum concentrations and could not be used for the DBR fabrication. Order was placed for a third wafer. The second wafer and Aerospace material were used, however, to train and to transfer the technology of fabrication to a new member of the technical staff, G. Evans, who joined Aerospace Corporation in April. He learned the photoluminescence and IMMA techniques, as well as ion milling and chemical etching. W. Soady, the technician who had done all the fabrication, left the department in July, while G. Evans continued to develop his skills in the fabrication steps, with Soady available for advice and Stoll available for technical direction. However, in September Stoll left the corporation, followed by Soady, and Evans was left fully responsible. He made rapid progress, and developed the techniques for etching down to the waveguide layer until they were reproducible and had good yields.

We received another wafer from Laser Diodes which proved to be suitable for DBR lasers and began the fabrication steps leading to DBR lasers.

Evans fabricated several runs of successful active/passive laser between November 1979 and March 1980. These devices were found to exhibit unique single mode properties, leading to a patent disclosure and publication, a preliminary version of which is found in Chapter VII. He was able to demonstrate that two separate runs, one by ion milling and one by chemical etching, both gave excellent operating diodes, and his experimental analysis techniques were sufficiently good that he could predict their properties.

It was discovered by January, 1980, that the grating fabrication procedures developed by Stoll and Soady would have to be refined to get sufficient efficiency for good DBR operation. From January to July, 1980, much effort went into redeveloping the grating fabrication procedures.

Fabrication of DBR lasers is now underway. That means combining the grating with the active-passive laser structure. The first set of this new batch of DBR lasers was fabricated in August, 1980, but did not work. Apparently the grating spacing was at the wrong wavelength. New DBR lasers are being fabricated at the present time with the appropriate grating spacing.

It is the consensus of opinion now that the bottleneck in fabrication of DBR lasers is availability of good quality epitaxial material. A collaborative effort is underway between Laser Diodes Laboratories and Aerospace Corporation and USC to develop good quality material with the right properties for DBR lasers. This involves careful investigation of aluminum concentration as well as flatness of the waveguide layers, since it is the lack of knowledge of the aluminum concentration which made the last run of DBR lasers unsuccessful.

## VI. AMPLIFIER STUDIES

In order to compare the advantages of using a phase-locked array of lasers to that of using amplifiers, it was proposed to embark on a study of laser amplifiers. This work resulted in a publication which has been accepted by Journal of Quantum Electronics. This chapter contains the text of this publication, entitled "Amplification in Cleaved Substrate Lasers" by M. B. Chang and E. Garmire.

### Abstract

Amplification has been measured in a DH GaAs regenerative amplifier. Both strong and weak signal regimes have been studied with measured gains as large as 170. A regime of coupling between the regenerative amplifier and laser source is also identified, resulting in a lowering of the threshold of the regenerative amplifier in the presence of an incident laser signal. Comparisons between the experimental results and the theoretical models show good agreement.

## Introduction

Amplification in GaAs lasers is attractive for applications in optical communications and integrated optical circuits. The first studies of GaAs amplifiers were of homostructure traveling wave amplifiers at 77°K [1-3]. Since the advent of the DH laser only a few studies have been conducted, such as the works of Schicketanz and Zeidler [4] on weak signal gains in traveling wave and regenerative amplifiers or Kishino, et.al. [5] on integrated laser amplifier devices. We report the amplification of a GaAs laser by a DH regenerative amplifier for both weak and strong signal regimes and also report a lowering of the oscillation threshold of the amplifier due to coupling with the laser source. These data were obtained with a simple cleaved-substrate device geometry.

The cleaved substrate geometry is shown in Fig. 1 and is similar to that used by Ksonocky and Cornely, [3]. The diodes were fabricated from wafers grown in our laboratory by standard LPE techniques. Stripe geometry contacts 50  $\mu\text{m}$  wide were applied and the diodes mounted p-side up for pulsed operation. Typical thresholds for individual cleaved diodes were between 0.75 and 0.85 amps, or a current density of about  $2.5 \text{ kA/cm}^2$ . The cleaved substrate laser amplifier pair was constructed from this material by first cleaving a chip 750  $\mu\text{m}$  long and 400  $\mu\text{m}$  wide. This chip was soldered to a gold-plated flexible metal plate using an indium alloy solder. The diode was then cleaved in half by nicking with a diamond scribe and subsequently bending the plate

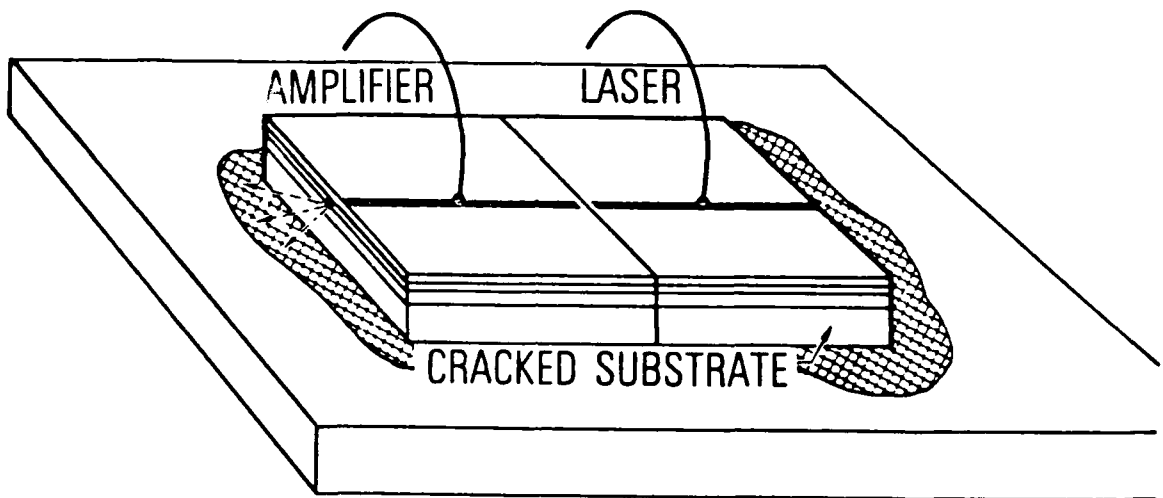


Figure 1. Diagram of geometry for the cleaved substrate laser-amplifier pair

very slightly. The resulting cleave formed a close-coupled laser-amplifier pair, with the amplifier already aligned to the laser. Unlike the amplifier of Kosonocky and Cornely, the output face of the amplifier was not lapped. As a result, this oscillator could be used either as a regenerative amplifier, for current levels below the lasing threshold, or as a laser, for current levels above the lasing threshold. Typical dimensions for the laser-amplifier pair were a laser length of 325  $\mu\text{m}$ , an amplifier length of 425  $\mu\text{m}$ , a striped contact width of 47  $\mu\text{m}$ , and a separation distance between the laser and amplifier of less than 2  $\mu\text{m}$ .

Amplification was measured through a monochromator with a resolution of 10  $\text{\AA}$  in order to monitor the gain at different wavelengths. The laser and amplifier were simultaneously pulsed with 100 nsec variable current pulses, and the output of the cleaved substrate device was monitored as a function of both the current to the laser portion and the current to the amplifier portion.

In general, the GaAs regenerative amplifier can be considered as a Fabry-Perot cavity with a nonlinear gain, a very difficult problem to solve analytically. However, in two regimes the gain may be considered independent of position inside the resonator. One regime occurs when the rate of carrier injection dominates the rate of change of population inversion due to absorption or emission (the so-called weak signal regime). The other regime occurs when the stimulated transitions dominate the carrier injection so that the populations in the upper and lower states equalize and the medium becomes transparent. This is the strong signal regime.

In both these cases the gain per unit length is constant inside the regenerative amplifier, and the regenerative amplifier gain may be derived in terms of the single pass gain: [6]

$$\frac{I}{I_0} = \frac{(1 - R)^2 G}{(1 - RG)^2 + 4 RG \sin^2 \theta} \quad (1)$$

where  $I$  is the light out of the regenerative amplifier,  $I_0$  is the light incident on the regenerative amplifier,  $R$  is the reflection coefficient for the amplifier, and  $G$  is the single pass gain of the amplifier. The quantity  $\theta$  is the accumulated phase shift due to a difference in the resonant frequencies between the laser and the regenerative amplifier. In our experiments, the resonant modes of the laser and amplifier varied with time, and Eq. (1) must be averaged over all values of  $\theta$ . This averaging gives the following result for regenerative amplifier gain:

$$\frac{I}{I_0} = \frac{(1 - R)^2 G}{1 - R^2 G^2} \quad . \quad (2)$$

This expression is valid in both the large and small signal regimes.

#### Strong Signal Regime

The strong signal regime occurs when the incident light intensity  $I_0$  is sufficiently large that absorption and stimulated emission processes are comparable and the medium becomes nearly transparent. The single pass (travelling wave) gain in the strong signal regime is [7]

$$G = \frac{I_{out}}{I_o} = 1 + \frac{1}{I_o} \left( S - \frac{N_s h \nu L}{\tau} \right) \quad (3)$$

where  $I_{out}$  is the intensity after a single pass through the amplifier,  $h\nu$  is the photon energy,  $\tau$  is the carrier relaxation time, and  $N_s$  is the carrier density determining the saturation intensity.  $S$  is the stimulated emission term which is related to current injection:

$$S = \eta \frac{J h \nu L}{e d}$$

where  $J$  is the current density,  $\eta$  is the internal quantum efficiency,  $L$  is the diode length,  $d$  the active region thickness, and  $e$  the electron charge. Note that the large signal gain approaches one as the incident light level increases. It can be seen from Eq. (3) that the signal out is equal to the signal in plus a contribution which is independent of input intensity and depends on the rate of excess carrier generation above that required to make the material transparent. This latter contribution is small, since the incident light level is large.

Combining Eqs. (2) and (3), the mode-averaged regenerative amplifier gain in the strong signal limit is

$$\frac{I}{I_o} = \frac{1-R}{1+R} - \frac{1}{I_o} \frac{1+R^2}{(1+R)^2} \frac{N_s h \nu L}{\tau} + \frac{1+R^2}{(1+R)^2} \frac{S}{I_o} \quad . \quad (4)$$

This gain is linear with respect to the current injected into the amplifier, which is contained in the factor  $S$ . This equation will be compared to the experimental results.

Typical data for strong signal amplification are shown in Fig. 2. The points represent experimental values and the lines represent a least squares fit of Eq. (4) to the data. The signal observed from the amplifier portion of the cleaved substrate device was measured as a function of the amplifier

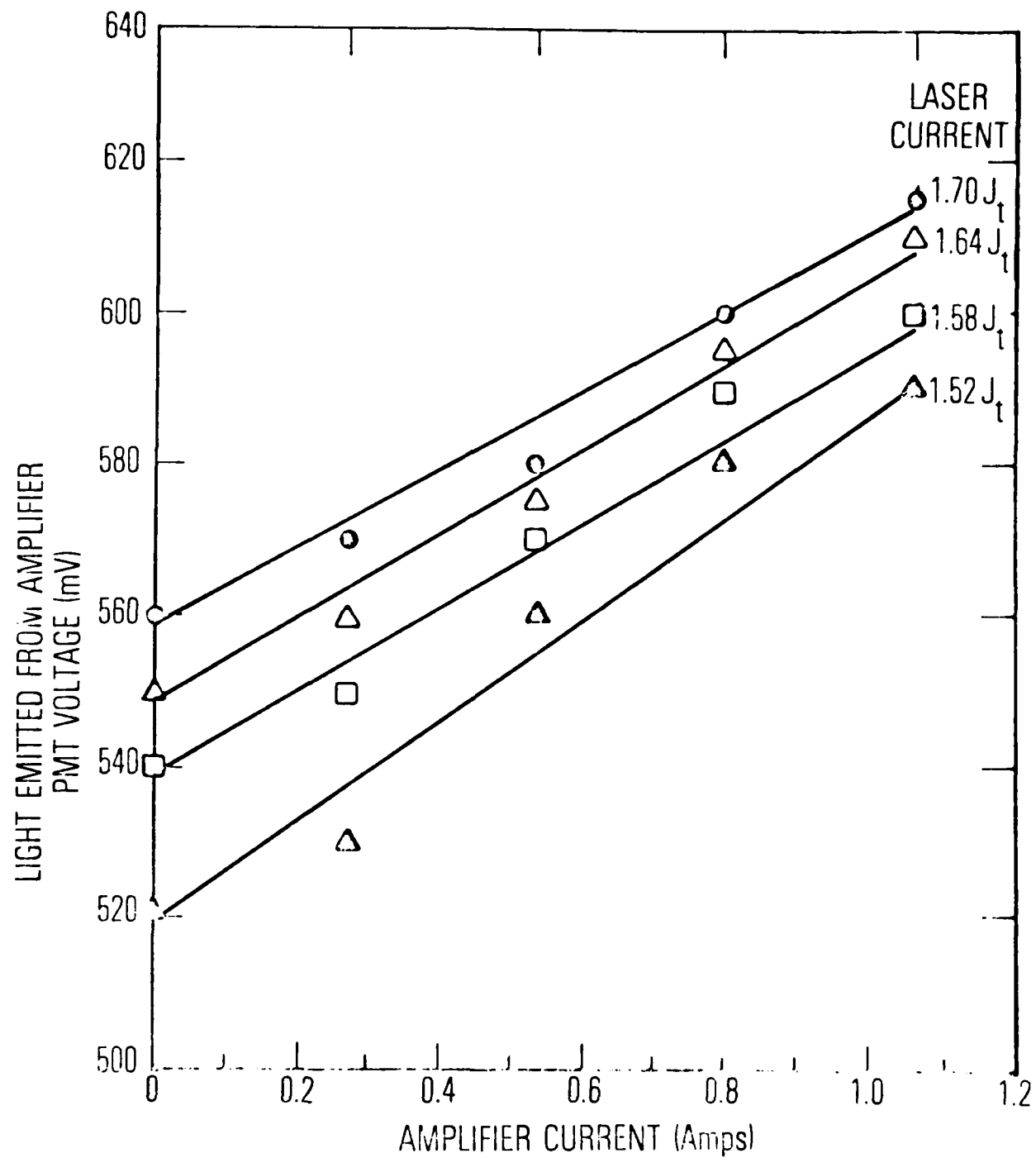


Figure 2. Emission from amplifier section of device L7C20 as a function of current applied to the amplifier, for several levels of current applied to the laser.

current, for several values of incident laser light. The strong signal regime was attained by operating the laser portion of the device far above its threshold current ( $J > 1.5 J_t$ ), where the laser signal was observed to be linear with its injected current. Figure 2 shows that the amplified signal is the expected linear function of the amplifier current. Because the exact reflectivity of the cleave is not known, and therefore the incident intensity is only approximately known, a rigorous comparison between experiment and theory could not be made. However, estimates can be made which allow comparisons and show agreement with the experimental results. It can be seen from Eq. (4) that the slope of the amplifier gain with current should be given by the incident intensity and the reflectivity.

An estimate of the power of the amplified light was made by comparing the photomultiplier signal with the signal of a photodiode calibrated by a power meter using a CW krypton laser source at 7880 Å. For a calibration factor of  $60 \text{ mV/mW}$ , an independently measured quantum efficiency of  $\gamma = 0.5$ , [9] and  $\lambda = 0.873 \text{ } \mu\text{m}$ , the slope of the amplifier gain with current was calculated to be 27. The measured slope was 52. Given the uncertainty of the calibration of the photomultiplier tube, we consider this excellent agreement.

The slope of Eq. (4) with respect to  $S$  or current is constant for various input intensities in the strong signal regime. This is seen in Fig. 2. The apparent discrepancy at  $1.52 J_t$ ,

the lowest current, is because the strong signal limit is no longer valid at this light level.

The intercept gives information as to the absorption of the amplifier, if the incident intensity is known. The intercept is the light transmitted through the amplifier with the amplifier turned off. This is equivalent to the incident light level minus the saturated absorption. Unfortunately we do not know accurately the incident light signal, since the apparent reflectivity of the interface between laser and amplifier depends strongly on the distance between the two facets, which we do not know with sufficient accuracy [3]. However, the fact that the intercepts in Fig. 2 are equally spaced as a function of the laser current is further evidence of strong signal amplification. For these laser currents the laser intensity is linear with respect to the laser current, as stated earlier.

It can be seen that the actual gain in the large signal limit is very small; the measured regenerative amplifier gain ( $I/I_0$ ) was roughly 1.1.

#### Weak Signal Amplification

The regime of weak signal amplification occurs when the dominant mechanism for carrier production is current injection. The gain of a traveling wave GaAs amplifier in the weak signal limit is [7]

$$G = \exp \left[ \left( g_o L \right) \left( \frac{S\tau}{N_s h v L} - 1 \right) \right] \quad (5)$$

where  $L$  is the amplifier length,  $g_o$  is the small signal loss coefficient in the absence of light. Equation 5 assumes that the GaAs laser can be represented by a two level system, and saturation of the gain with injection current is ignored. Combining Eqs. (2) and (5), the weak signal gain of a mode-averaged regenerative amplifier is

$$\frac{I/I_o}{1} = \frac{(1-R)^2 \exp \left( g_o L \left( \frac{S}{N_s h L} - 1 \right) \right)}{1-R^2 \exp \left( 2 g_o L \left( \frac{S}{N_s h L} - 1 \right) \right)} \quad (6)$$

When  $RG \ll 1$ , the regenerative gain approximates that of a traveling wave amplifier and is exponential with respect to the amplifier current. Only near the oscillation threshold for the regenerative amplifier ( $RG = 1$ ) does the effect of regeneration become appreciable.

In order to attain the weak signal regime with the close-coupled cleaved substrate device (which did not allow an external attenuator to be placed between the laser and amplifier), we used a device which had two oscillation wavelengths in the laser, one which coincided with the peak of the amplifier gain and one at which the amplifier gain per unit length was small. These frequencies correspond to two different oscillation filaments in the wide-stripe geometry.

Small signal amplification was observed at the wavelength for which the amplifier gain per unit length was small. To separate the regimes, the amplification was measured as a function of wavelength through a monochromator.

Data was taken at a fixed laser current, above threshold. The amplifier output was measured as a function of amplifier current at both the wavelength of the peak amplifier gain (8768 Å) and at the wavelength of the stronger laser line (8729 Å), where the amplifier gain per unit length was small. The data is shown in Fig. 3. It can be seen that although the amplifier gain per unit length was much smaller at 8729 Å, the amplified signal was almost as large as the saturated signal at 8768 Å. The amplified signal at 8768 Å is best explained by a coupled oscillator model, and is discussed separately in the next section.

The quantity of interest to those who intend to use amplifiers for practical applications is the system gain. This is given by

$$G_S = \frac{P_{LA} - P_A}{P_L} \quad (7)$$

where  $P_{LA}$  is the light power emitted when current is applied to both the laser and amplifier,  $P_A$  is the power emitted when current is applied only to the amplifier, and  $P_L$  is the power emitted only when the current is applied to the laser. The data for the weak signal amplifier system is shown as the points in Fig. 4. This presentation of the data enhances the anomaly around 0.7 Å. At this current, the amplifier gain at 8729 Å starts to become super-linear. However, at a slightly larger current, another frequency with a larger gain 8768 Å, begins to lase and, in the competition for carriers,

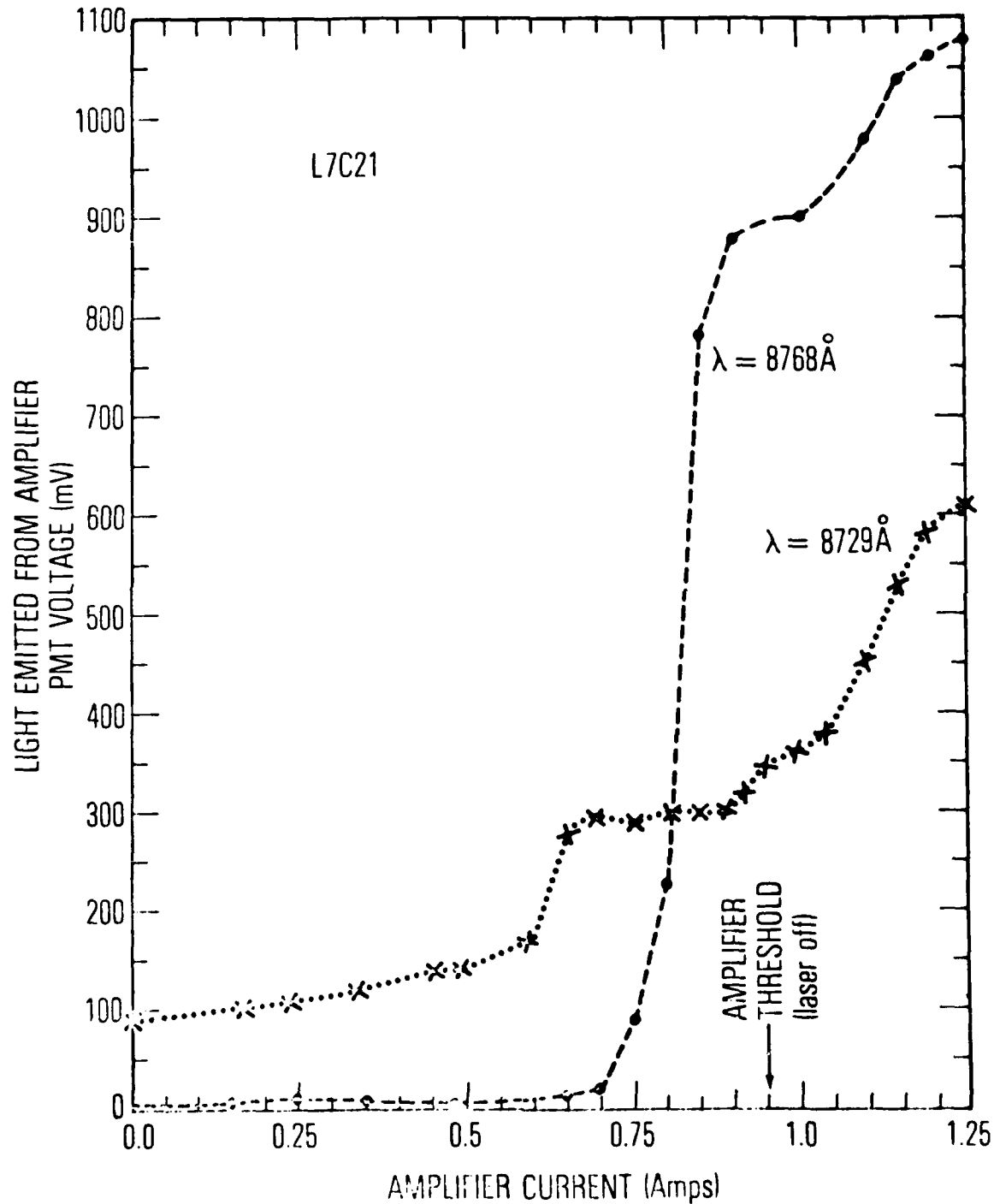


Figure 3. Emission from amplifier section of diode L7C21 as a function of amplifier current, for two different wavelengths. The shorter wavelength exhibits weak signal amplification; the longer wavelength exhibits strong signal amplification.

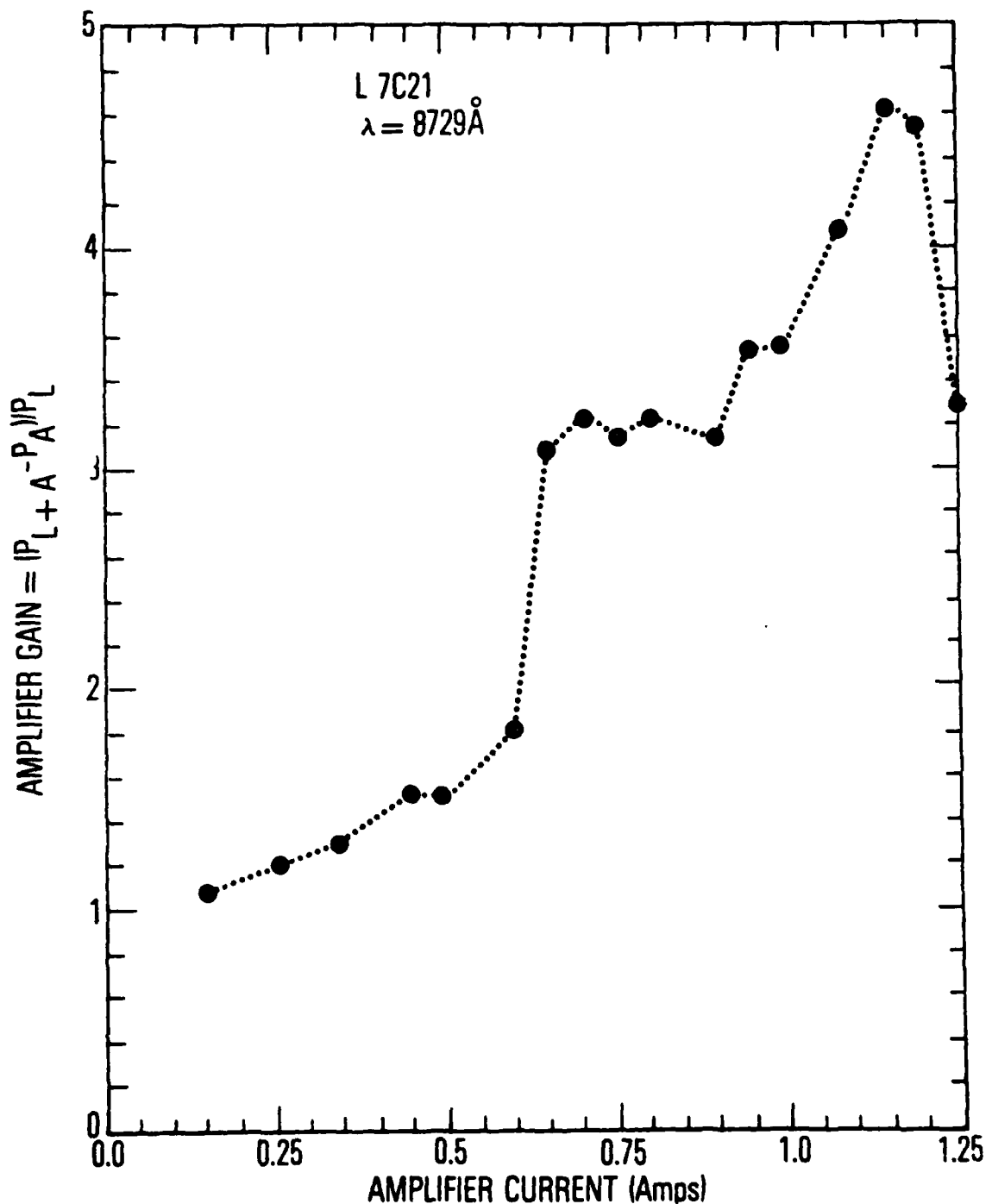


Figure 4. Amplifier gain as a function of amplifier current for diode L7C21 at  $8729\text{\AA}$ .

quenches the oscillation at 8729 Å (shown in Fig. 3). It is only at larger currents, when the gain at 8768 Å saturates, that the line at 8729 Å begins to lase. This occurs at 1.25 A resulting in the drop in gain seen in Fig. 4.

The amplifier gain has been fit by two curves. The solid curve is the regenerative amplifier fit from Eq. (6) while the dotted curve is the exponential fit of the traveling wave amplifier (Eq. 5). The regenerative amplifier model yields a slightly better fit. From this fit, the small signal absorption coefficient of the unpumped amplifier,  $\alpha = g_o$ , was determined to be  $14 \text{ cm}^{-1}$ . This value is comparable to those published [9] and indicates that we have good agreement between experiment and theory for the regenerative amplifier in the small signal limit.

An additional comparison between the experimental curve and the theoretically predicted curve can be made in terms of the amplifier threshold. In the small signal limit, the gain is

$$\alpha = g_o \left( \frac{S}{LN_s h} - 1 \right) .$$

This equation can be rewritten in terms of measurable quantities using the threshold equation,  $g_{th} L = -\ln R$ , and the proportionality between the injection rate,  $S$ , and the injected current.  $\xi^* = \frac{J}{J_{th}} (2L - \ln R) - \alpha L$

Using the measured value for the threshold current, this equation can be compared with theory. For  $\alpha = 14 \text{ cm}^{-1}$ ,  $L = 0.043 \text{ cm}$ ,

$R = 0.32$ , and a threshold current of 1.1 amps, we obtain  $g_L = 1.5 \mathcal{I} - 0.60$  where  $\mathcal{I}$  is the applied amplifier current. The coefficient for the amplifier current, 1.5, is in good agreement with the experimentally measured value of 1.14.

Further comparison between experiments and theory can be made by considering the order of magnitude of the saturation density,  $N_s$ . From the fit to equation (6),  $\frac{\alpha S \tau}{N_s h v} = 1.14 \mathcal{I}$ ,

where  $\mathcal{I}$  is the applied current. Using the definition of  $S$ ,  $\alpha \tau / (edw) = 1.14$ . For stripe widths  $w = 47 \mu\text{m}$ ,  $d = 0.26 \mu\text{m}$ ,  $\eta = 0.5$ , and

$\tau = 1 \text{ ns}$  [10], the saturation density is  $N_s \sim 10^{17} \text{ cm}^{-3}$ . This density is comparable to the doping density of the active layer and lends confidence to our interpretation.

#### Coupled Oscillators

The data at 8768 Å shown in Fig. 3 is better fit by a coupled oscillator model than by the theory of regenerative amplification. Regeneration plays a dominant role in this regime, since it was observed that the amplifier section began to oscillate at 0.95 amps, in the absence of incident light from the laser section. In addition, coupling between the laser and amplifier sections caused an apparent lowering of the threshold for the amplifier section in the presence of light from the laser section. This can be seen in Fig. 5, in which the amplifier system gain, defined by Eq. (7), is plotted as a function of current to the amplifier section. It can be seen that

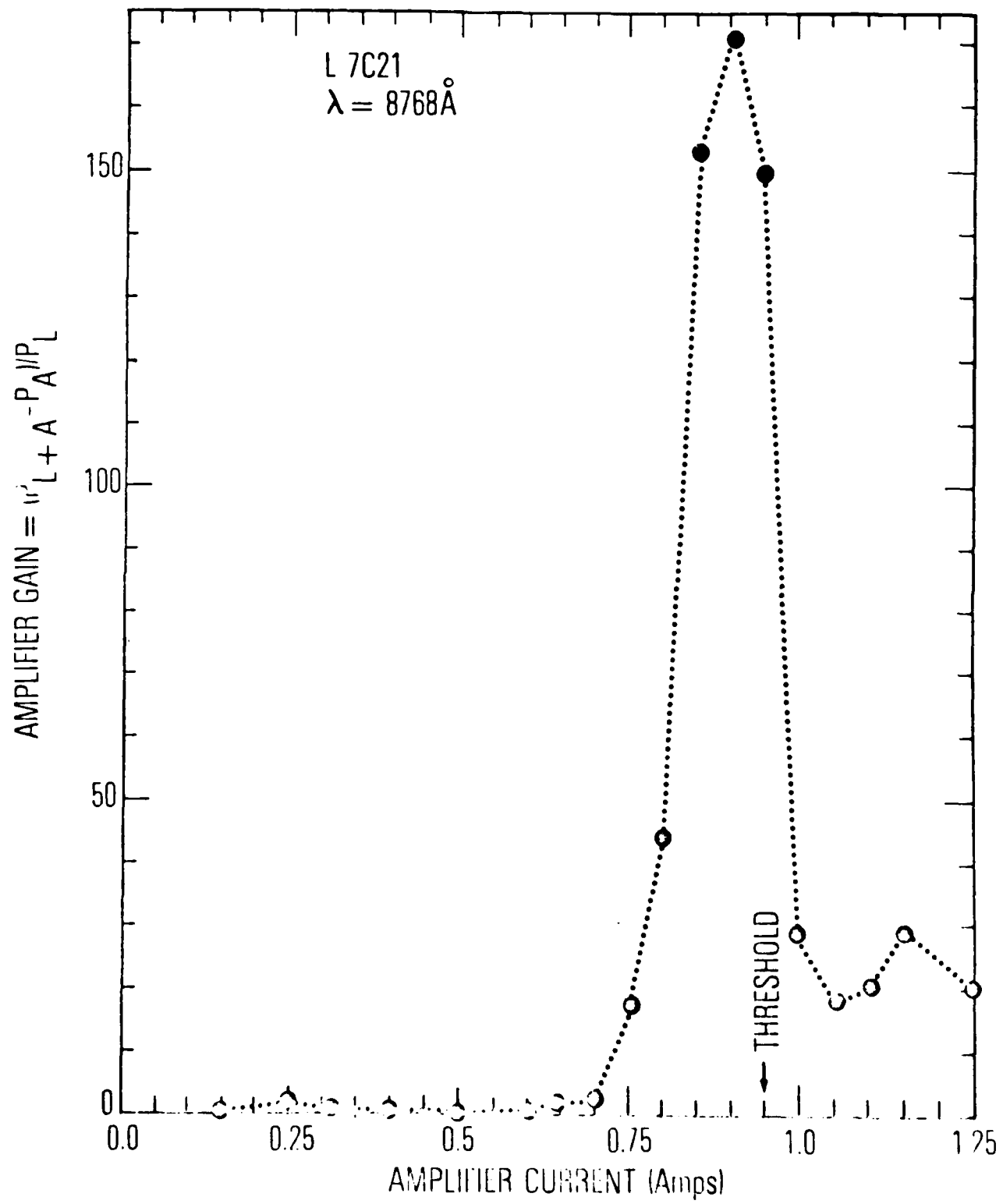


Figure 5. Amplifier gain as a function of amplifier current for diode L7C21 at  $8768\text{\AA}$ .

very high gains are measured just below the threshold for oscillation in the absence of current applied to the laser section. The apparent dramatic decrease in gain is due to the onset of self-oscillation in the amplifier section. Below this threshold the large apparent gain is the result of a lowered threshold for the coupled oscillator system.

Comparison with theory requires the study of coupled oscillators, a model in which the amplifier section is above oscillation threshold. The way in which the two oscillators are coupled can be seen from plotting the threshold for oscillation of the coupled laser-amplifier system as a function of the current applied to the laser section and the current applied to the amplifier section. This is shown in Fig. 6. It can be seen that the presence of some current in the amplifier section has a slight effect on the device threshold, decreasing it somewhat. However, it can be seen that the presence of current in the laser region has a strong effect on the device threshold. If there were no interaction between the laser and amplifier, the threshold current should be constant. If the laser-amplifier acted as a single laser, however, the curve should be a straight line. The experimental curve shows that the light from a neighboring oscillator causes an effective lowering of the threshold.

The lower threshold can be explained by an increase in the effective reflectivity [10]. The effect of the second laser cavity is to act as if, instead of a reflectivity due to Fresnel reflections only, there is an effective reflectivity which

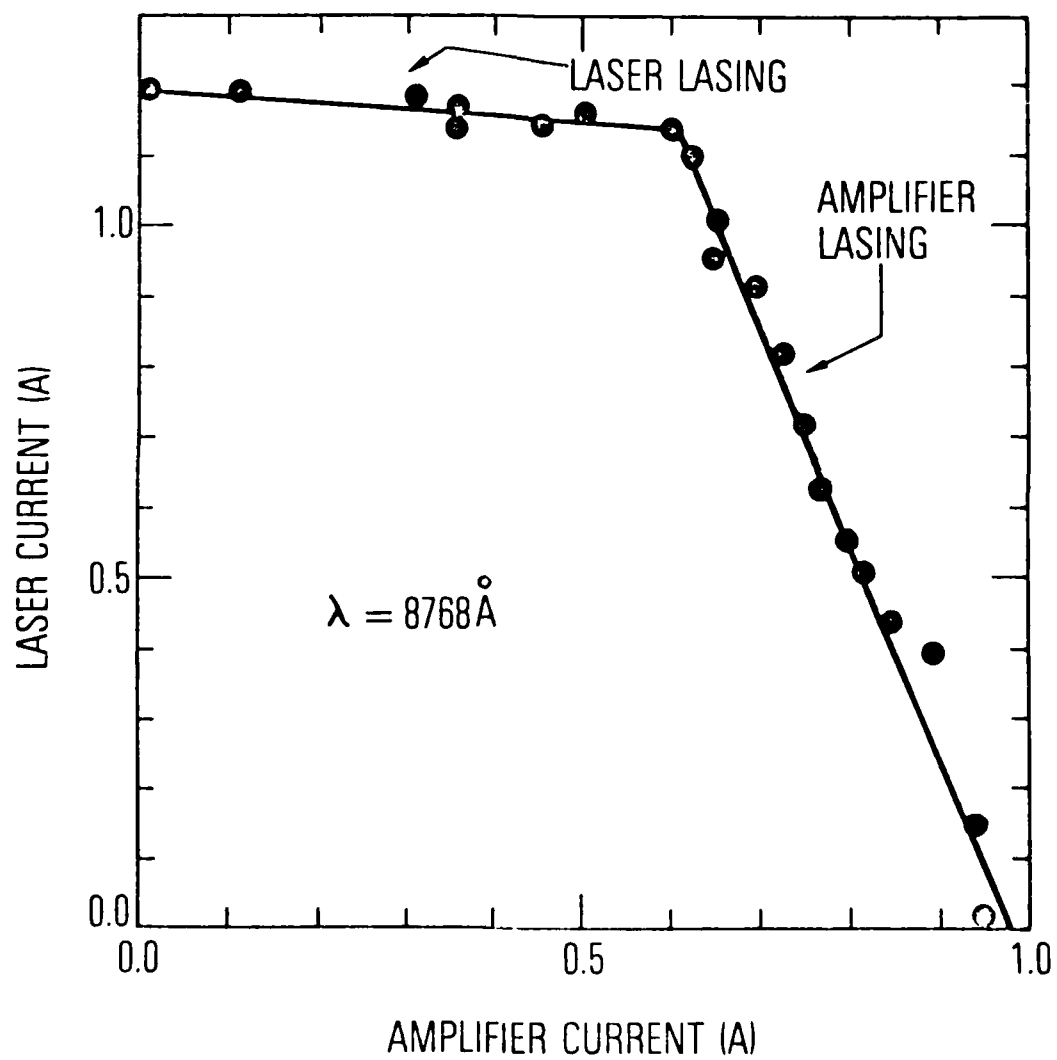


Figure 6. Threshold of coupled oscillator emission as a function of both current to the laser portion and current to the amplifier portion.

includes light from the neighboring oscillator. Only that fraction of the neighboring light which is coherent with the indigenous light of the diode has an effect upon the effective reflectivity. The threshold condition for diode 1 may then

be written as  $I_1 = R e^{\frac{2g_1 L_1}{R\{1 + P_2(e^{\frac{g_2 L_2}{2}} - 1)\}}}$

where  $g_j$  is the gain per length in diode  $j$ ,  $L_j$  is the length of diode  $j$ ,  $R$  is the reflectivity of a cleaved facet, and  $P_2$  is a constant measuring the fractional change in the reflectivity due to coherent coupling. This equation can be rewritten in terms of the injected currents,  $I_1$  and  $I_2$ ,

$$0 = b_1 I_1 + \ln(R A_1) + \frac{1}{2} \ln(1 + P_2 (e^{\frac{a_2 I_2}{2}} - 1)) \quad (8a)$$

$$0 = b_2 I_2 + \ln(R A_2) + \frac{1}{2} \ln(1 + P_1 (e^{\frac{a_1 I_1}{2}} - 1)) \quad (8b)$$

where  $b_j$  is the gain coefficient in diode  $j$  at threshold,  $A_j$  is the loss coefficient in diode  $j$ , and  $a_j$  is the coherent gain coefficient in diode  $j$ . Equation (8a) is the threshold equation for diode 1 while Eq. (8b) is the threshold equation for diode 2. When  $\exp(b_j I_j)$  is much greater than 1 and  $P_j$  is larger than 1, (as in the case observed), the threshold equations reduce to the linear equations,

$$0 = b_1 I_1 + \ln(R A_1 P_2) + \frac{1}{2} a_2 I_2 \quad (9a)$$

$$0 = b_2 I_2 + \ln(R A_2 P_1) + \frac{1}{2} a_1 I_1 \quad (9b)$$

The excellent fit of Eq. (9) to the data is shown in Fig. 6.

In conclusion, we have measured the strong and weak signal gains for a DH regenerative amplifier. As in the case of homostructure traveling wave amplifiers, the strong signal gain was small and limited by saturation. The weak signal gain was shown to be much larger, particularly just below the lasing threshold of the amplifier, where the gain was as large as 170. Finally, coupling between the lasers and amplifier resulted in lower threshold currents for both the laser and amplifier.

The authors would like to acknowledge the able assistance of J. Osmer in crystal growth and of M. Ziegler in diode preparation.

#### REFERENCES

1. J.W. Crowe and R.M. Craig, *Appl. Phys. Lett.*, vol. 4, 57 (Feb. 1964) "Small-Signal Amplification in GaAs Lasers".
2. J.W. Crowe and W.E. Ahearn, *IEEE-J. Quantum Electron.*, vol. QE-2, 283 (Aug. 1966) "Semiconductor Laser Amplifier".
3. W.F. Kesonocky and R.H. Cornely, *IEEE J. Quantum Electron.*, vol QE-4, 125, (Apr. 1968) "Semiconductor Laser Amplifier".
4. D. Schicketanz and G. Zeidler, *IEEE J. Quantum Electron.*, vol. QE-11, 65, (Feb. 1975), "GaAs - DH Lasers as Optical Amplifiers".
5. K. Kishino, Y. Suematsu, K. Utaka and H. Kawanishi, *J JAP* 17 (3), 589, (1978), "Monolithic Integration of Laser and Amplifier/Detector by Twin-Guide Structure".
6. D. Röss, Lasers, Light Amplifiers, and Oscillators, Academic New York 1969.
7. F. Stern, Proc. Physics of Quantum Electronics Conf., N.Y. McGraw-Hill, 1966, "Saturation in Semiconductor Absorbers & Amplifiers of Light".
8. H.S. Sommers, Jr., *Appl. Phys. Lett.*, vol. 32, 547, (May 1978), "Algorithm for Measuring the Internal Quantum Efficiency of Individual Injection Lasers".
9. G.H.B. Thompson, G.D. Henshall, J.E.A. Whiteaway, and P.A. Kirkby, *J. Appl. Phys.*, vol 37, 1501, (April 1976)., "Narrow-Beam Five-Layer (GaAl)As/GaAs Heterostructure Lasers with Low Thresholds and High Peak Power".
10. C.H. Gooch, GaAs Lasers, John Wiley & Sons, New York 1969.

## VII . SINGLE MODE THREE-MIRROR ACTIVE/PASSIVE GaAs LASERS

This reports single longitudinal mode lasers operating at current levels up to 1.5 times threshold, using integrated optics techniques to form a three-mirror laser diode which contains a long active cavity and a short passive cavity. The additional mirror results from an abrupt etch step into the waveguide layer of large optical double heterostructure laser, forming a short passive region. Conditions on geometry and operating temperature which result in single mode operation are outlined.

Methods of fabricating single longitudinal mode GaAs lasers have typically involved DFB or DBR lasers,<sup>1,2</sup> single longitudinal mode resulting from development of a single spatial mode<sup>3-7</sup>, or coupling between active and passive waveguides<sup>8-10</sup>. Other techniques include the use of very short lasers,<sup>11</sup> a bent-guide structure<sup>12</sup> and use of an external cavity.<sup>13</sup> The structure demonstrated here utilizes an integrated optics equivalent of an external cavity in which a third mirror introduces a short passive cavity into the laser diode by the use of an abrupt etch step. This approach does not require grating fabrication, epitaxy over etched substrates, controlled diffusion or unusual electrode stripe geometries. All processing is applied to planar, large optical cavity epitaxial material.

Single longitudinal mode lasers are reported at 1.5 times threshold, using the active/passive three-mirror arrangement shown in Fig. 1. The epitaxial structure is the similiar to that which has been used for DBR lasers.<sup>2</sup> Protecting the active laser cavity area with a mask, an abrupt step in the waveguide layer was made by removing all layers in the passive region through the active laser layer and partially removing a portion of the passive waveguide layer. The etching was accomplished with ion milling on some samples, with selective chemical etch on others, and both techniques gave excellent results. This abrupt etch step causes a reflection from the waveguide discontinuity, forming a third mirror within the diode (the other two are the usual cleaves at the ends of the diode). This third mirror forms a laser with a long active activity and a short passive cavity.

An example of the single mode output is shown in Fig. 2, in which weak sidebands may be observed at spacings equal to both the spacing of the passive cavity ( $20\text{ \AA}$ ) and of the active cavity ( $1.7\text{ \AA}$ ). Linewidths of typically  $1\text{ \AA}$  were

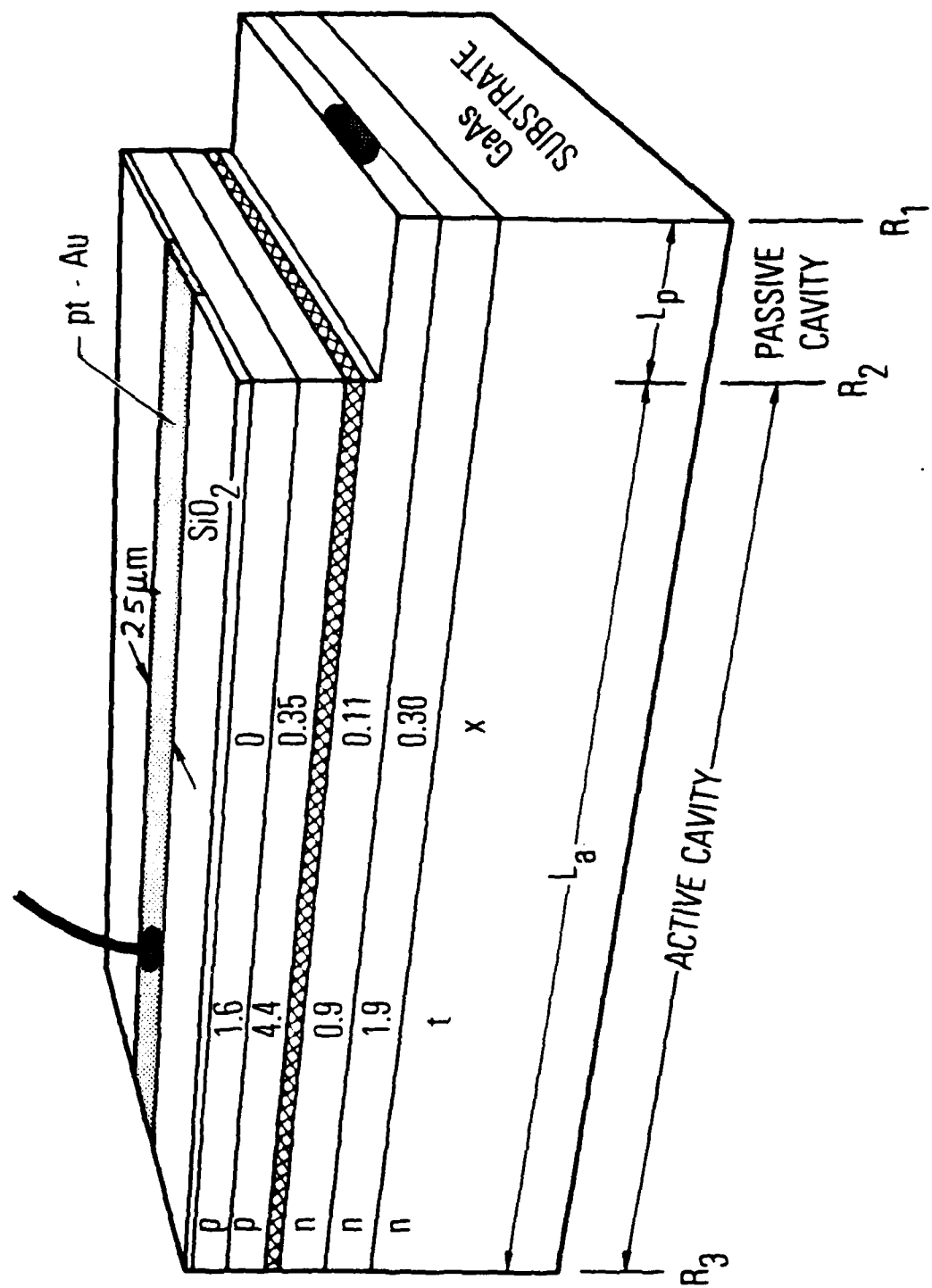


Figure 1. Geometry for two-cavity single longitudinal mode lasers which were fabricated and tested. The epilayer structure is described by  $p, n$  representing majority carriers,  $t$  representing layer thickness and  $x$ , representing the fraction of AlAs in each layer. The active layer is cross-hatched,  $0.12\mu\text{m}$  thick and contains 7% AlAs. The abrupt etch step in the waveguide layer causes a reflection  $R_2$ . The length of the active cavity,  $L_A$ , and of the passive cavity,  $L_p$  were varied over a wide range.

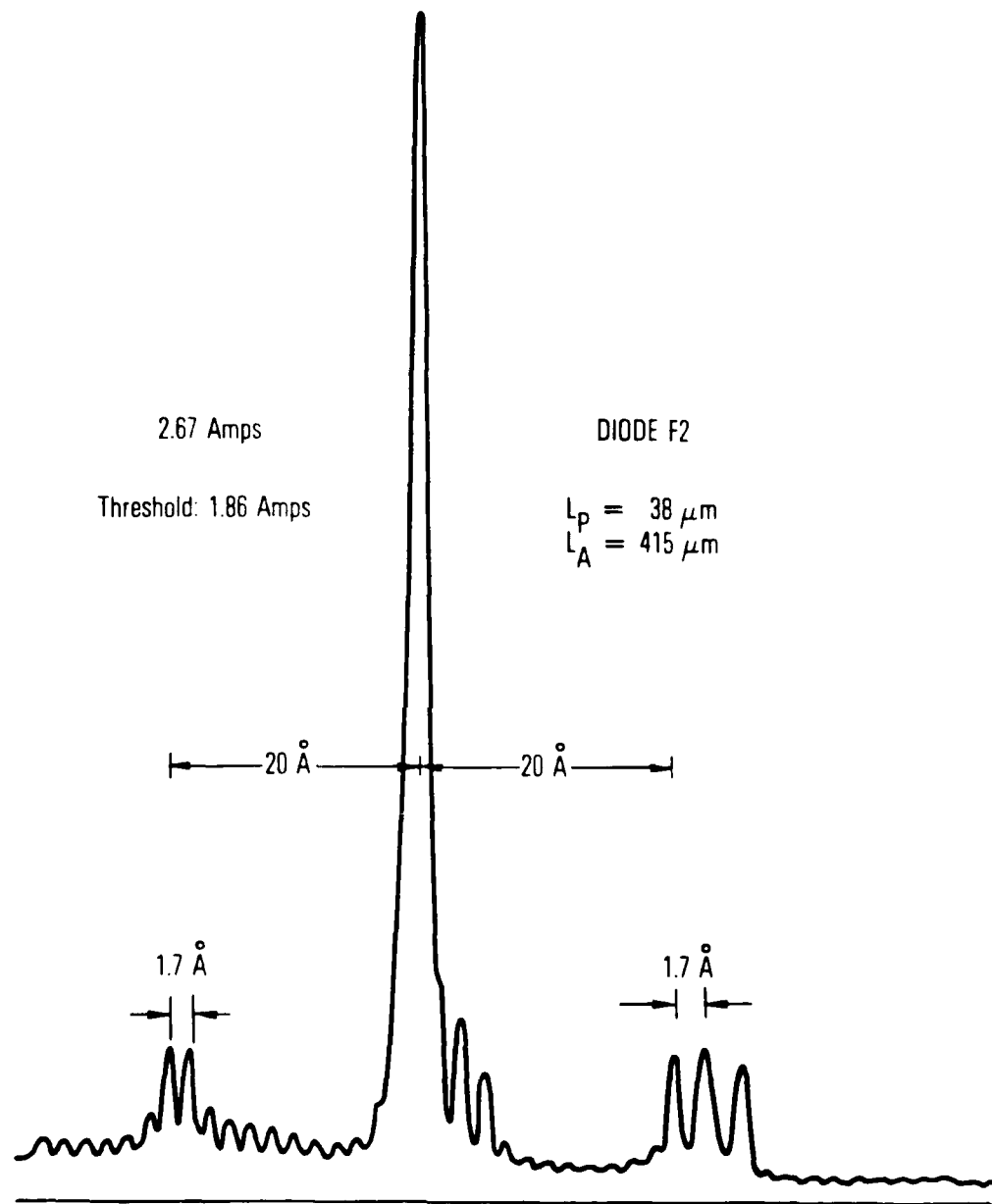


Figure 2. Single mode operation of diode F2, at a current level 44% above threshold. Closely spaced modes of the active cavity and more distantly spaced modes of the passive cavity can be seen in the background.

measured, and were due to thermal chirping, since the lasers were operated pulsed, without heat sinks, p-side up.

Single mode operation occurs as a result of the overlap of the resonance for transmission of the active cavity with the peak in the reflectivity of the passive cavity, and the mutual overlap of both these resonances with the peak of the gain line. The requirement that all three effects overlap puts criteria on the cavity dimensions. However, since the peak of the gain spectrum, and the optical path lengths within the diode are temperature sensitive, it is possible to vary the device temperature to ensure that all three criteria are achieved. We found that single mode operation depends on temperature. Requirements on the operating temperature to ensure single mode operation will be discussed below.

A wide range of geometries for the active/passive structures resulted in single mode operation. The table shows data on several lasers and the range of currents over which single mode operation was observed. With favorable geometries, all of the diodes fabricated had a range of single mode operation, proving that the active/passive design is both repeatable and reproducible. The table includes measured threshold currents, for stripe contacts 25  $\mu\text{m}$  wide. The high thresholds were due to non-optimum epilayer structure, and were consistent with two-mirror Fabry-Perot diodes fabricated from the same material. This indicates that neither the etch step, nor a short passive region significantly contributes substantially to the loss in the diode. Calculations indicate that it should be possible to obtain cw operation from these active/passive structures when the epilayer structure is optimized.<sup>14</sup>

The table includes theoretical estimates for the mode-selective properties of the active/passive structure in the various geometries. Mode selection is determined by the fractional decrease in gain at the adjacent mode of the passive cavity,  $(g-g_0)/g_0$ , and the fractional decrease in reflectivity of the passive cavity at the adjacent mode of the active cavity,  $\delta R/R$ . These quantities were determined as follows.

Estimates for the decrease in gain were obtained by fitting measured fluorescence spectra near the peak of the emission with a Gaussian model:

$$g = g_0 \exp \left( - \frac{\lambda - \lambda_0}{\Delta \lambda} \right)^2 \quad (1)$$

TABLE: PARAMETERS OF SINGLE MODE LASERS

| Diode # | L <sub>P</sub><br>μm | L <sub>A</sub><br>μm | Threshold<br>amps | Single Mode<br>Operation |           | SR/R<br>% | (g - g <sub>0</sub> )/g <sub>0</sub><br>% |
|---------|----------------------|----------------------|-------------------|--------------------------|-----------|-----------|---|
|         |                      |                      |                   | % Above Threshold        | Threshold |           |   |
| F6      | 27                   | 275                  | 1.8               | >25                      |           | 4         | 14  |
| F7      | 25                   | 275                  | 2.4               | 10                       |           | 3         | 14  |
| F2      | 38                   | 415                  | 1.8               | 50                       |           | 3         | 8   |
| F1      | 38                   | 415                  | 2.0               | 30                       |           | 3         | 8   |
| Eb3     | 96                   | 484                  | 2.7               | 10                       |           | 15        | 1.6                                       |
| Eb4     | 100                  | 484                  | 2.4               | 6                        |           | 15        | 1.3                                       |
| Eb1     | 95                   | 485                  | 2.7               | 3                        |           | 15        | 1.6                                       |
| F4      | 20                   | 310                  | 4.0               | MMA                      |           | 1.5       | 17  |
| F8      | 10                   | 310                  | 2.1               | MMA                      |           | 0.4       | 73  |
| Ea4     | 200                  | 470                  | 2.3               | 10                       |           | 86        | 0.3                                       |
| Ea1     | 200                  | 470                  | 3.7               | MMP                      |           | 86        | 0.3                                       |
| Ea2     | 200                  | 470                  | 3.0               | MMP                      |           | 86        | 0.3                                       |
| Ea3     | 200                  | 470                  | 2.8               | MMP                      |           | 86        | 0.3                                       |

We found that within 200Å of the emission peak, the fluorescence could be fit by  $\Delta\lambda = 2\text{\AA}$ , while the peak of the gain line,  $\lambda_0$ , shifted approximately 2 Å/degree.

The value of  $\delta R/R$  introduced by the etch step was estimated by using a crude model based on an abrupt etch step in a hollow metal waveguide.<sup>15</sup> For a single mode waveguide with an abrupt fractional decrease in waveguide height,  $\epsilon$ , the reflectivity is given by

$$R_2 = \left\{ \frac{(2 - \epsilon)^2 - 4p^2(1 - \epsilon)}{(2 - \epsilon)^2 + 4p^2(1 - \epsilon)} \right\}^2 \quad (2)$$

where  $p = (\sin \epsilon \pi) / \epsilon \pi$ .

Typical numbers indicate that a 50% decrease in waveguide height at the etch step causes a reflectivity of 22% (and transmission of 78%). The determination of more accurate numbers would require computer calculation of the guided mode in each region and match boundary conditions at the etch step.<sup>16</sup>

The reflectivity of the etch step can also be inferred from the ratio between the outputs from the active and passive ends. Consider the passive cavity as a typical Fabry-Perot interferometer, in which the transmission is<sup>17</sup>

$$T = (1 + F \sin^2 \theta)^{-1}, \quad (3)$$

where  $\theta = 2\pi n L_p / \lambda$  ( $n$  is the refractive index in the waveguide), and  $F$  is the finesse of the cavity:

$$F = \frac{4R}{(1 - R)^2} \quad (4)$$

where  $R = \sqrt{R_1 R_2}$ . Here  $R_1$  is the reflectivity of the cleave. The laser will operate at maximum reflectivity for the passive cavity where  $\theta = \pi/2$  and  $T = (1 + F)^{-1}$ . Typically twice the intensity was emitted from the active as from the passive end, independent of the length of the passive cavity. Since the transmission of the cleave at the active end is 70%, the transmission of the passive cavity is 35%. Using this value for  $T$  we obtain  $F = 1.86$ ,  $R = 0.26$

and  $R_2 = 0.22$ . This is the same as the estimated reflectivity for a 50% abrupt change in waveguide height.

To estimate the effect of the passive cavity on the spectral output of the diode laser, assume that the temperature is chosen to match the resonance of the active cavity with the peak reflectivity of the passive cavity. The fractional decrease in reflectivity of a Fabry-Perot from its peak value to that of the next mode of the active cavity can be written as

$$\frac{\delta R}{R} = \frac{\sin^2 \phi}{1 + F \cos^2 \phi}$$

where  $\phi = 2\pi n L_p (v_o - v_1)/c$ , where  $v_o$  is the frequency of light at the peak reflectivity and  $v_1$  is the frequency of the next cavity mode. Since  $\frac{v_o - v_1}{c} = \frac{1}{2\pi n L_p}$ ,  $\phi = \pi L_p / L_A$ .

From the table it can be seen that a number of geometries result in single mode operation, substantially above threshold, even with only 2% decrease in reflectivity or 5% decrease in gain at adjacent modes. This is confirmation that the lasers are homogeneously broadened and that the addition of the passive cavity eliminates longitudinal mode hopping or spatial hole burning. A more careful analysis of the relative roles of the two mode selectivities may provide further information on the operation of stripe geometry lasers which do not have a single transverse mode.

There are two temperature requirements to obtain single mode operation. First, the ability to tune the gain curve so that its peak is centered on a passive cavity resonance. Since these resonances are at most  $40\text{\AA}$  apart, and the peak in the gain spectrum shifts typically  $2\text{\AA}/\text{deg}$ , this means that a temperature tuning of  $10^\circ\text{C}$  is sufficient to match gain peak and passive resonance. An additional factor to consider is that the peak of the gain shifts also with drive current, as the band fills. This means that the optimum temperature may vary somewhat with current drive. The second temperature requirement is on the stability of the temperature to maintain a single mode of the active cavity. Since the cavity modes are separate by at least  $2\text{\AA}$ , a temperature control of a quarter of a degree should suffice to maintain the active and passive cavities in resonance. These are reasonable requirements on temperature control, and we found no problem in maintaining single mode operation over long periods of time.

If the peak of the gain curve is exactly halfway between the two modes of the passive cavity, it is possible to obtain a two-mode laser, as shown in Fig. 3. Such a laser may be useful for multiplexing applications. Temperature tuning this device will turn it into a single mode laser. Single longitudinal mode active/passive cavity lasers have been demonstrated using a wide range of geometries. Additional improvements in design should lead to single longitudinal mode operation up to at least two times threshold and eventually to cw operation. This will involve optimizing dimensions for the active and passive cavities, optimizing the epilayer structure and varying the reflectivities of the cleaves and etch step. Finally, there is a wealth of opportunities for improvement by using an additional etch step to fabricate a three-cavity active/passive laser.

DIODE F6  $L_p = 27 \mu\text{m}$   $L_A = 275 \mu\text{m}$

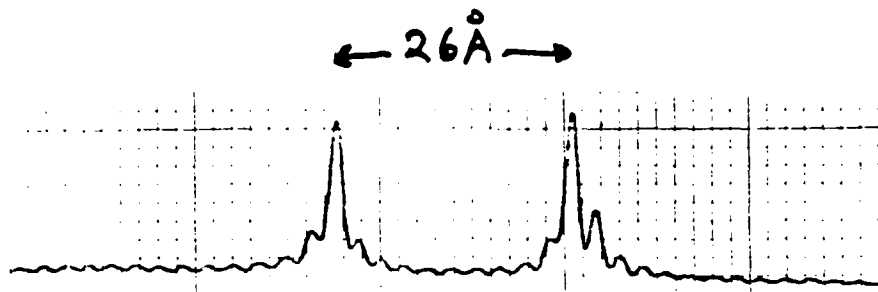


Figure 3. Two-frequency spectrum obtained when temperature is tuned so that the gain peak is halfway between the resonances of the passive cavity.

#### REFERENCES

1. M. Nakamura, K. Aiki, J. Umeda, A. Katzir, A. Yariv, H. W. Yen, IEEE J. Quantum Electr. QE-11 436 (1975).
2. M. K. Shams, S. Wang, Appl. Phys. Lett. 33, 170 (1978).
3. W. Susaki, T. Tanaka, H. Kan, M. Ishii, IEEE J. Quantum Electr. QE-13 (1977).
4. M. Nakamura, K. Aiki, N. Chinone, R. Ito, J. Umeda, J. Appl. Phys. 49, 4644 (1978).
5. W. T. Tsang, R. A. Logan, M. Illegems Appl. Phys. Lett. 32 311 (1978).
6. D. Botez, Appl. Phys. Lett. 33 872 (1978).
7. R. D. Dupuis, P. D. Dapkus Appl. Phys. Lett. 33 725 (1978).
8. Y. Suematsu, K. Kishino, T. Kambayashi IEEE J. Quantum Electr. QE-13 619 (1977).
9. D. R. Scifres, R. D. Burnham, W. Steifer, Appl. Phys. Lett. 32 658 (1978).
10. J. L. Merz, R. A. Logan Appl. Phys. Lett. 32 661 (1978).
11. N. Matsumoto, IEEE J. Quantum Electr. QE-13 560 (1977).
12. N. Matsumoto, S. Ando Jap. J. Appl. Phys. 16 1697 (1977).
13. R. Salathe Appl. Phys. 20 1 (1979).
14. M. B. Chang, E. Garmire, Appl. Optics 19, 2370, 1980.
15. R. A. Waldren Theory of guided Electromagnetic Waves (Van Nostrand

Reinhold, New York, 1969) p. 490.

16. J. L. Merz, R. A. Logan, A. M. Sargent IEEE J. Quantum Electr. QE-15 72 (1979).
17. J. Born and E. Wolf, Principles of Optics (Pergamon Press, New York, fifth edition, 1975) p. 327.

## VIII. Plans for the future

The collaboration between USC and The Aerospace Corporation is intended to continue, as progress is made toward the development of the high brightness lasers. However, as a result of the last two-and-a-half years of research, we realize that progress toward the high brightness laser will be much slower than originally anticipated. The speed of the development is currently limited by personnel and equipment constraints at The Aerospace Corporation. The company has provided sufficient internal funds that the program will continue to develop. The level of funding is sufficient to fund two principal investigators, who are now G. Evans and T. Gallanowicz. In addition, J. Niesen, R. Cordero, and A. Chase are members of the technical staff who are involved. J. Osmer continues to be responsible for the crystal growth, and there are three technicians, who assist in fabrication and evaluation studies. Professor Garmire continues to consult on the direction of the programs, in all phases of the fabrication, and design.

The more modest time-scale for achievement expects DBR fabrication routinely and the first devices including a beam expander to be achieved by the end of FY'81. Near term goals include major improvements in epitaxial growth and in application of contacts. The etch to the DBR structure and grating fabrication are apparently under control. The fully integrated high brightness laser is not currently in Aerospace Corporation's plans.

The high brightness laser will be fabricated with a parallel effort at USC. In December, 1980, the Center for Laser Studies will be moving to a new laboratory, which will include a clean room devoted to diode fabrication, and a separate room for epitaxial growth. The equipment to furnish those laboratories is on order.

Professor Garmire started the epitaxial growth system at Caltech and at The Aerospace Corporation, and now intends that research into epitaxial growth will take place at USC. This will allow a parallel effort which should solve some of the problems of obtaining flat enough layers for DBR fabrication. A full-time graduate student will be assigned to the particular problem of ensuring that the layers are sufficiently flat. We expect that collaboration between USC and The Aerospace Corporation will continue, and that etch and grating fabrication will continue there, as long as their techniques continue

to give high quality results. In exchange, USC will provide epitaxial wafers to them. We also expect USC to have high quality contacting procedures, as a graduate student at USC has already had good success in this area. The collaboration envisaged will be a trade of goods and services, as well as knowledge between Aerospace and USC, but each program will be funded separately and will be directly responsive to the needs of the contractors.

The program at USC could progress at a funding rate comparable to that of the past, but without the subcontract to The Aerospace Corporation. We expect that we shall be able to fabricate DBR lasers within the first year of such a contract, and fabricate the 45° HBL during the second year of the contract. During the first year, USC will concentrate on crystal growth, and Aerospace will do much of the fabrication. During the second year, the grating fabrication will be set up at USC in parallel to Aerospace.

Nothing in the research which has gone into this contract has led us to believe that the high brightness laser is an unworkable concept. We are as positive as ever about its potentialities, but considerably more realistic about the time scale in which devices can be delivered. While we believe the first HBL lasers can be fabricated within two years, we believe it will be five years before an efficient, low threshold, five unit array will be available.

We encourage PML/TRADE to continue funding a research effort in this area, as we believe it will further the technology which will eventually make the high brightness laser reality. We are proud of the research effort which we have undertaken. It has led to considerable new knowledge and to the publications listed in the enclosed table.

TABLE - PUBLICATIONS SUPPORTED ON THIS CONTRACT

| <u>Title</u>   | <u>Authors</u>                           | <u>Journal (Conference)</u>   |
|--|--|---|
| 1. "Distributed Bragg Deflector: A multi-functional Integrated Optical Device" | H. Stoll                                 | Applied Optics <u>17</u> , 2562 (1978)  |
| 2. "High Brightness Lasers Using Integrated Optics"                            | H. Stoll                                 | Proc. SPIE <u>139</u> 113 (1978), also presented at the Symposium on Guided Wave Optics, 1978 |
| 3. "Bragg-Effect Polarizer/Analyzers and Lens-Less Waveguide Beam Expansion    | H. Stoll, W. Soady                       | Presented at the Integrated Optics Conference, 1980   |
| 4. "Optimally Coupled, GaAs Distributed Bragg Reflection Lasers"               | H. M. Stoll                              | IEEE Trans. Integ. Circuits, 1980   |
| 5. "Optimum Epilayer Structures for Integrated Optics Lasers"                  | M. B. Chang, E. Garmire                  | Applied Optics <u>19</u> , 2370 (1980).   |
| 6. "Optical Coupling Between Parallel Diodes"                                  | M. B. Chang, E. Garmire                  | Submitted to Applied Optics   |
| 7. "Fabrication Techniques for DBR Lasers"                                     | G. Evans, E. Garmire, H. Stoll, W. Soady | Presented at the American Vacuum Society annual meeting, 1980                                 |
| 8. "Amplification in Cleaved Substrate Lasers"                                 | M. B. Chang, E. Garmire                  | IEEE J. Quantum Electr. September, 1980   |
| 9. "Amplification in Cleaved Substrate Lasers"                                 | M. B. Chang, E. Garmire                  | Presented at the Integrated Optics Conference, 1980   |
| 10. "Self-Amplification of TM Light in a TE Polarized Laser Diode"             | M. B. Chang, E. Garmire                  | Submitted to Applied Optics   |
| 11. "Single Mode Three-Mirror Active/Passive GaAs Lasers"                      | E. Garmire, G. Evans, J. Nelson          | Submitted to Applied Physics Letters  |